Full length article

Numerical study on the progressive collapse of cable-stayed columns due to cable loss

Michał Kierat [a], Fabio Freddi [b],*

[a] *Ove Arup & Partners, 8 Fitzroy Street, London W1T 4BJ, UK*
[b] *Dept. of Civil, Environmental & Geomatic Engineering, University College London, London WC1E 6BT, UK*

ARTICLE INFO

ABSTRACT

Extreme loading events, such as accidents, impacts, or malicious attacks, may generate local failures that can propagate to subsequent elements, leading to the ultimate collapse of a structure. Research into progressive collapse has mainly focused on structures characterised by high levels of redundancy (*e.g.,* moment-resisting frames). Conversely, little attention has been given to low-redundant structures (*e.g.,* cable-stayed), which may be characterised by higher vulnerability to progressive collapse due to limited alternative load paths. This paper focuses on a distinct form of cable-stayed structures, *i.e.,* cable-stayed columns, evaluating their robustness by considering a cable loss scenario and identifying measures able to reduce the risk of progressive collapse. A variety of bay/branch configurations with fixed and pinned cross-arms were investigated through Finite Element (FE) models developed in OpenSees, accounting for material and geometric non-linearities. An extensive parametric study was initially performed to evaluate the influence of variables on the load-carrying capacity. Cable loss scenarios were successively simulated in non-linear quasi-static and dynamic analyses. Incremental Dynamic Analyses (IDAs) were also conducted to estimate Dynamic Increase Factors (DIFs) for mid-node displacement, axial, and reaction forces (proxy for load-carrying capacity) for several non-dimensional slenderness ratios. In all cases, significant reductions in the buckling load were recorded, with dynamic effects amplifying the columns' response. The present paper sheds light on the performance and design of cable-stayed columns under cable loss scenarios. The results show that, whilst additional branches in the geometric configuration were found to be beneficial in maintaining capacities under cable loss, the appropriate selection of cross-arm profile and its bending stiffness were vital in reducing the risk of collapse.

1. Introduction

Progressive collapse is the process of local failure of a structural element initiating the progressive failure of other elements, leading to the total or partial collapse of the structure [1]. This can be caused by various factors, such as designers underestimating or failing to predict the full range of loads acting on the structure accurately, improper or neglect of maintenance, or, as a result of extreme events (*e.g.,* blasts, impacts, malicious attacks). Several well-known progressive collapse disasters of different origins, such as the Ronan Point Building, London, UK, in 1968 [2], the Murrah Federal Building, Oklahoma City, USA, in 1995 [3], and the World Trade Center, New York, USA, in 2001 [4], triggered extensive studies into this research area. Since the 1940s, diverse aspects of the problem have been researched by performing component- and large-scale experimental tests considering different structural typologies and materials such as steel [*e.g.,* 5,6], reinforced concrete [*e.g.,* 7,8], precast concrete [*e.g.,* 9,10], and steel-concrete composite [*e.g.,* 11–13] structures. Several studies also addressed the development and application of simplified [*e.g.,* 13–16] and advanced [*e.g.,* 17–22] modelling strategies to advance knowledge and promote the development of design strategies against progressive collapse [*e.g.,* 23–25]. These studies enhanced the understanding of structural responses to these scenarios and enabled the definition of strategies that are now incorporated into design guidelines and codes [*e.g.,* 26–28]. Seeking alternate load paths, ensuring the presence of tying forces, focusing on key element design, compartmentalisation, and analysis of collapse occurrence risk are now internationally recognised methods for designing against progressive collapse [29,30]. However, most of these studies and determined approaches focused on structural systems usually characterised by high levels of redundancy (*e.g.,* reinforced concrete

or steel moment-resisting frames), whilst low-redundant structures (*e.g.,* trusses or cable-stayed systems), which could be more vulnerable to progressive collapse, have received less attention.

Among others, cable-stayed systems represent one typology of low-redundancy structures. The growing demand for large and unobstructed spaces within the built environment has led to an increase in the use of cable-stayed structures. They can efficiently achieve larger spans compared to conventional alternatives, allowing for greater freedom in architectural design. These systems are widely used in iconic structures worldwide, typically where occupancy levels are significant, such as stadia or convention centres, and commonly within bridges; examples are shown in Fig. 1. Cable-stayed structures rely on the high tensile strength of cables to carry loads axially; since most members are designed to act in tension, dealing with the buckling phenomenon is typically limited to the design of key compressive components [31]. These systems are optimised with a minimal number of elements, which consequently limits alternative load paths and makes them particularly vulnerable to abnormal or extreme accidental loads [32]. There is often insufficient redundancy within these systems; the failure of a single element could lead to the failure of subsequent elements and, potentially, the entire structure. It is crucial to acknowledge that the design process of any structural system aims to strike an acceptable balance between safety concerns and structural/material/carbon/cost optimisation, also including considerations related to the system's robustness, *i.e.,* its ability to withstand accidental actions without undergoing damage that could be deemed disproportionate [27]. Only a few research studies have investigated progressive collapse within cable-stayed structures, with a primary focus on bridges [*e.g.,* 33]. Exposed cables can be vulnerable to various unpredictable actions. Moreover, cable rupture can induce dynamic loading impulses, amplifying the structure's response. The collapse of the Morandi Bridge in Genoa, Italy, in 2018 [34] is an iconic example where the failure of a single strand propagated to the progressive global failure of a significant part of the structure. In 2019, the Nanfang'ao tied-arch bridge in Thailand [35] collapsed due to corrosion despite its multi-suspension-cable design. In 2020, the Arecibo Telescope in Puerto Rico [36] suffered a catastrophic collapse; the dynamic effects of an initial cable failure likely led to an increase in fatigue cracks in the remaining cables, ultimately causing multiple cables to snap. These examples highlight the lack of robustness within cable-stayed structures and their vulnerability to progressive and disproportionate collapse.

A simple representation of cable-stayed systems can be found in the form of cable-stayed columns (Fig. 2). They are characterised by high structural efficiency and are of architectural interest, usually being left exposed. The use of tensioned cable systems increases the load-carrying capacity of the columns compared to conventional equivalents, allowing the use of much slender columns. Some examples of the application of this system include [37] the Chiswick Business Park in London, UK (Fig. 2a), the Mont-Cenis Academy in Herne, Germany, the Grande Arche in Paris, France, the Frick Chemistry Lab in Princeton, USA (Fig. 2b) and the Algarve Stadium in Algarve, Portugal. Cable-stayed columns are composed of 3 primary elements: *1)* the main column (typically circular hollow profile); *2)* horizontal cross-arms (usually circular bars or circular hollow sections), rigidly fixed or pinned to the main column; and *3)* the cable-stays. These components can be combined in various configurations and are differentiated by the number of branches (*i.e.,* number of cross-arms in the transverse plane) and bays (*i.e.,* number of cross-arm groups in the longitudinal axis). More complex systems can be formed with the addition of secondary stays, as shown in Fig. 2a. These columns have been relatively well studied in their own right. Initial research dates back to the 1960s when the prestressing of columns with tension ties was considered [39,40]. Buckling was studied

throughout the 1970s and 80s, looking in detail at pre-tensioning and imperfection effects [41–44]. In the last 20 years, a significant amount of research into cable-stayed columns has been conducted, with most of these studies focusing on post-buckling behaviour and stability [45–51]. In addition, research has included experimental [52–57] and optimisation [58–62] studies, as well as the development of design guidelines [63]. Some studies also investigated different failure modes of such structures, including the effect of fire on the stays [64,65]. Finite Element (FE) models developed for the abovementioned research have mainly relied on static approaches. To the author's knowledge, only one research work focused on the dynamic response of cable-stayed columns [66]. In this work, the authors investigated the dynamic response of a single geometry to an impact load applied to the top of the column and evaluated the Dynamic Increase Factor (DIF) for central node displacement. The results suggested that the dynamic effects could nearly double the lateral central node displacement, with larger DIFs being observed when cables were prestressed compared to no system prestress. These findings are insightful to the system's dynamic behaviour; however, alternative geometries and parameter values ought to be studied further to determine their effects, not only on displacement response but also on internal forces.

This paper sets out to investigate the optimisation-robustness relationship in cable-stayed columns. First, the range of case studies, the general FE modelling approach, and its validation are outlined. A variety of bay/branch configurations with fixed and pinned cross-arms are investigated by FE models developed in OpenSees [67], accounting for material and geometric non-linearities. Initial sensitivity studies and an extensive parametric analysis seek to understand the multi-parameter relationship to load-carrying capacity and material requirement, considering full system geometries (*i.e.,* the undamaged structure). Subsequently, the behaviour of the system under a cable loss scenario (*i.e.,* the damaged structure) is investigated by performing non-linear quasi-static and dynamic analyses. The analysis procedures for cable loss simulation are described along with the consideration of Engineering Demand Parameters (EDPs). Incremental Dynamic Analyses (IDAs) are conducted to estimate Dynamic Increase Factors (DIFs) for mid-node displacement as well as axial and reaction forces for several non-dimensional slenderness ratios. This study aims to shed light on the dynamic behaviour of cable-stayed columns under cable loss, identifying key aspects that affect their robustness along measures to protect the system against progressive collapse.

2. Case studies and finite element (FE) modelling

To investigate the influence of various properties on the capacity and progressive collapse resistance of cable-stayed columns, a FE model was developed in OpenSees [67] capable of simulating a range of geometrical configurations. Different FE types and procedures were used to model geometrical and material non-linearities and carry out quasi-static and dynamic analyses. The modelling strategy was validated against previous theoretical and experimental results for a case study column. A sensitivity study was conducted to evaluate critical parameters and select appropriate variables and geometries for the more extensive multi-parameter sensitivity analysis.

2.1. Geometrical configurations

The study focused on cable-stayed 1- and 2-bay columns with 3- and 4-branches. Additional configurations with 6-branches were also analysed as geometries that could perform better under the cable loss scenario. The range of considered configurations is depicted in Fig. 3a. Although fixed cross-arm connections are most widely used in practice,

Fig. 1. Iconic examples of cable-stayed and cable-supported structures. (a) Renault Centre,[11] Swindon, UK; (b) Serreria Bridge,[22] Valencia, Spain; (c) Millenium Dome,[33] London, UK; (d) David L. Lawrence Convention Center,[44] Pittsburgh, USA.
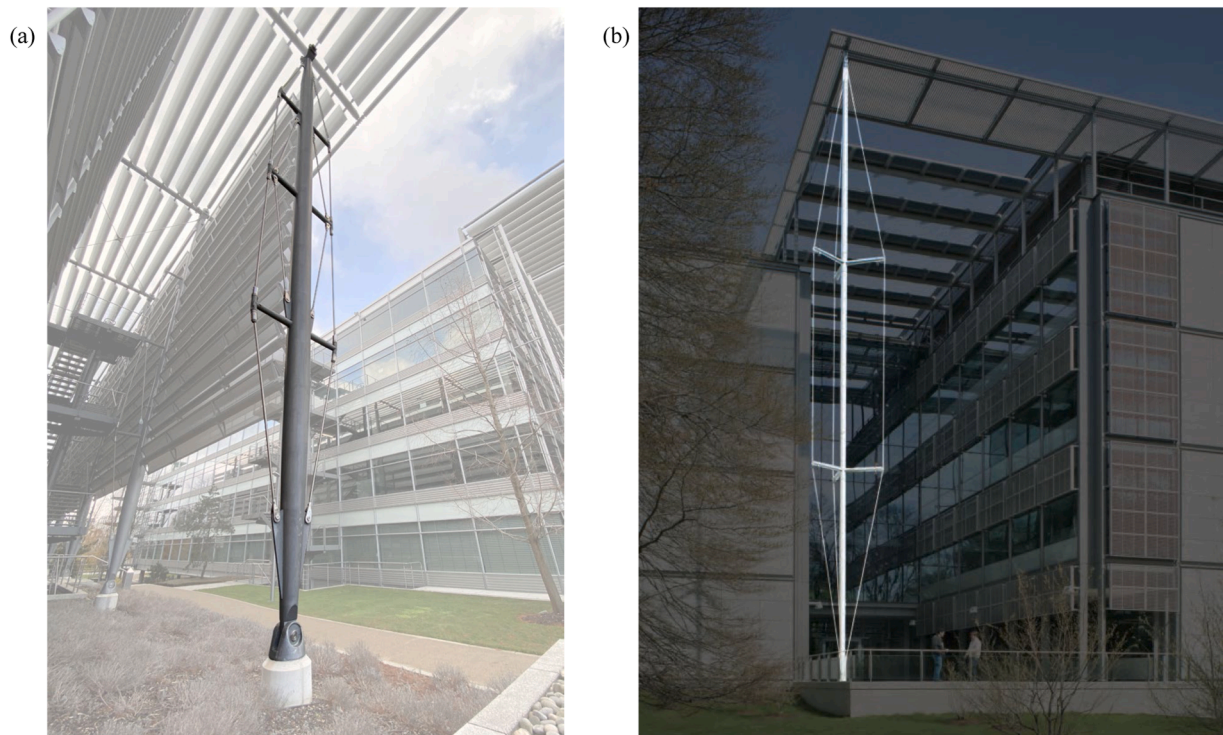

Fig. 2. Application of cable-stayed columns for solar-shading roof canopies. (a) Chiswick Business Park, London, UK; (b) Princeton University's Frick Chemistry Laboratory, Princeton, New Jersey, USA (Image adapted from [38]).

the prospect of simpler fabrication and assembly of pinned connections prompted both fixed and pinned scenarios to be considered.

Table 1 specifies the examined parameters. Properties for the baseline model (Table 1-I) were defined according to those in Wadee et al., [63]. Additional geometries were selected for the multi-parameter analysis (Table 1-II); these were identified based on the initial sensitivity study (discussed in Section 2.4), and values were chosen considering conceivable limits and common sizes. A total of 67,500 unique
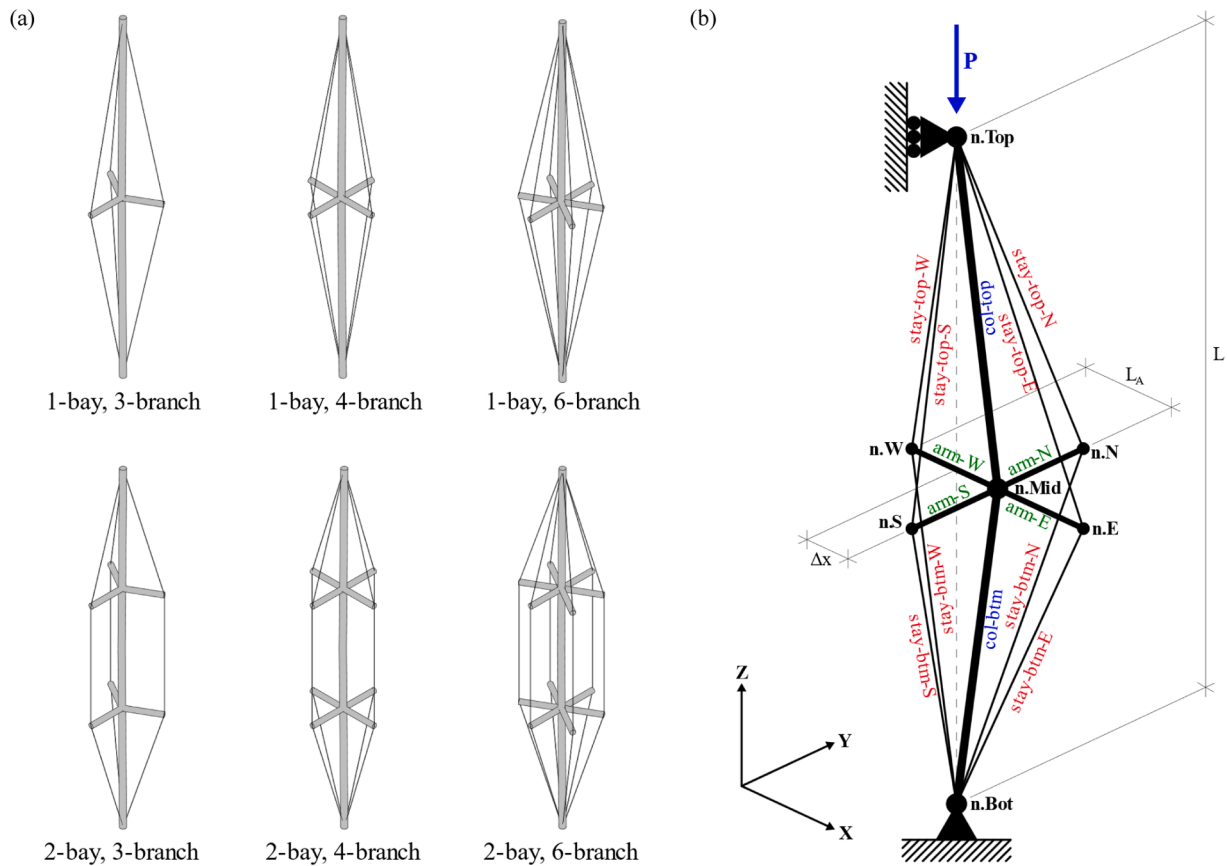
Fig. 3. Cable-stayed column geometry modelling approach: (a) considered geometric configurations, (b) diagram of OpenSees [67] model geometry for the 1-bay, 4-branch case; L – column length, L_a – cross-arm length, Δx – X-axis imperfection.

Table 1
Model parameters and values used in baseline model (I) and multi-parametric analysis (II).

Element	Symbol	Property	Unit	(I) Baseline	(II) Parametric Analyses	
				Value	Values	No. of values
Column	L	Column length	[m]	**20.0**	3, 5, 10, 15, 20, 30	6
	e_0/L	Imperfection level	[-]	**1/200**	1/200	1
	d_C	Column outer diameter	[mm]	**168**	100, 125, 150, 200, 300	5
	t_C	Column wall thickness	[mm]	**8**	3, 5, 10, 15, 20	5
Cross-arms	L_A	Cross-arm length	[m]	**0.5**	0.3, 0.5, 1.0	3
	d_A	Cross-arm outer diameter	[mm]	**140**	140	1
	t_A	Cross-arm wall thickness	[mm]	**8**	8	1
Stays	d_S	Stay diameter	[mm]	**12**	5, 8, 12.5, 16, 20	5
	T_0	Stay pre-tension	[kN]	**8**	0, 10, 20, 50, 80	5
numBays		No. of bays	[-]	**1**	1, 2	2
numBranches		No. of branches	[-]	**4**	3, 4, 6	3
					TOTAL Configurations	**67,500**

models were generated for the multi-parametric analysis.

2.2. Finite element (FE) modelling

A FE model of the column system was built up as illustrated in Fig. 3b and could be easily adapted for different model configurations and parameters (*i.e.,* number of bays, branches, column length, etc.). The model considered a pinned base connection, and the top node free to rotate about all axes and vertically translate (*i.e.,* acting as a vertical roller). The axial force was applied by a concentrated point load at the top node. A sway of Δx at the mid-height node of the column was included to account for geometric imperfections, as well as to induce the symmetric buckling mode. The column and cross-arm members were modelled by a distributed plasticity approach (*i.e.,* the

'*nonlinearBeamColumn*' element in OpenSees [67]) with a '*patch circ*' [67] fibre section with five integration points. The '*Steel01*' material was used for these elements, with yield strengths assumed as 355 and 420 MPa, respectively, for the column and cross-arms. A strain-hardening ratio of 0.002, Young's modulus of 210 GPa and shear modulus of 81 GPa were assigned for both materials. The '*Corotational*' transformation option was used to account for the geometric non-linearities. The stays were modelled as '*corotTruss*' elements, with Young's modulus in tension unchanged but set to 1 GPa under compression to reflect that the stays are not able to carry compressive loads; a small value was required to ensure convergence of results. A tensile strength limit was not specified, but results were post-processed to eliminate cases where stay forces exceeded their ultimate strength. Pre-tensioning was implemented using '*InitStrainMaterial*' with the initial strain equal to T_0 /

($A_{stay} \times E$), where T_0 is the pre-tensioning force, A_{stay} is the cross-sectional area of the stay, and E is the stay's tensile Young's modulus.

2.3. Model validation

The OpenSees model was validated against theoretical and experimental results to gain confidence in the modelling strategy. Quasi-static analyses with an incrementally increasing load were performed. The fundamental column geometry (i.e., without any stays) was analysed to verify global buckling. This was done by varying the column length on the baseline model (properties in Table 1-I). Fig. 4a shows the OpenSees results compared against theoretical material yield and Euler buckling. In addition, the numerical results expressed in terms of the non-dimensional slenderness ratio and normalised in the form of the buckling reduction factor in Fig. 4b were compared against the limits of the

buckling curves defined by Eurocode 3 [68], showing good agreement.

To validate the non-linear model of the full system geometry, including the pre-tensioned cable-stay system, the results of the OpenSees model were compared against experiment results from Osofero et al., [53]. Parameters were modified to reflect the conditions of the tested column assemblies from the experiment. Fig. 5a and 5b show the comparison of two cases of identical geometry for symmetric buckling with different values of stay pre-tensioning. The maximum values of the load-carrying capacity produced by the OpenSees model were found to be within a reasonable deviation of the experimental results; the lateral displacements of the mid-height node were also found to be within a comparable range. A further comparison was conducted against the parametric numerical results from Osofero et al., [48], which investigated the influence of the stay pre-tensioning force and column imperfection on system behaviour. Fig. 5c illustrates that the numerical models show similar trends, further increasing the confidence in the
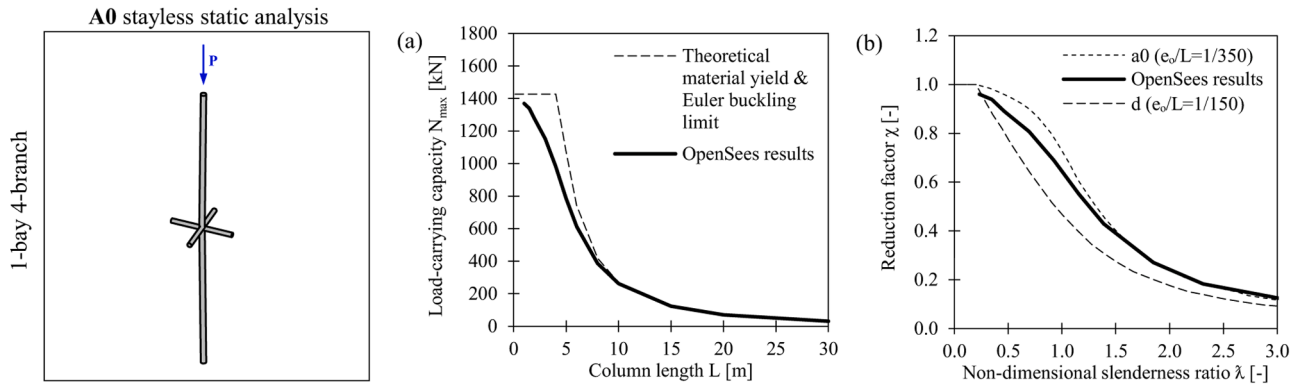

Fig. 4. Model validation of the fundamental column geometry: (a) comparison of numerical results against theoretical limits; (b) comparison of the normalised results against Eurocode buckling curves.
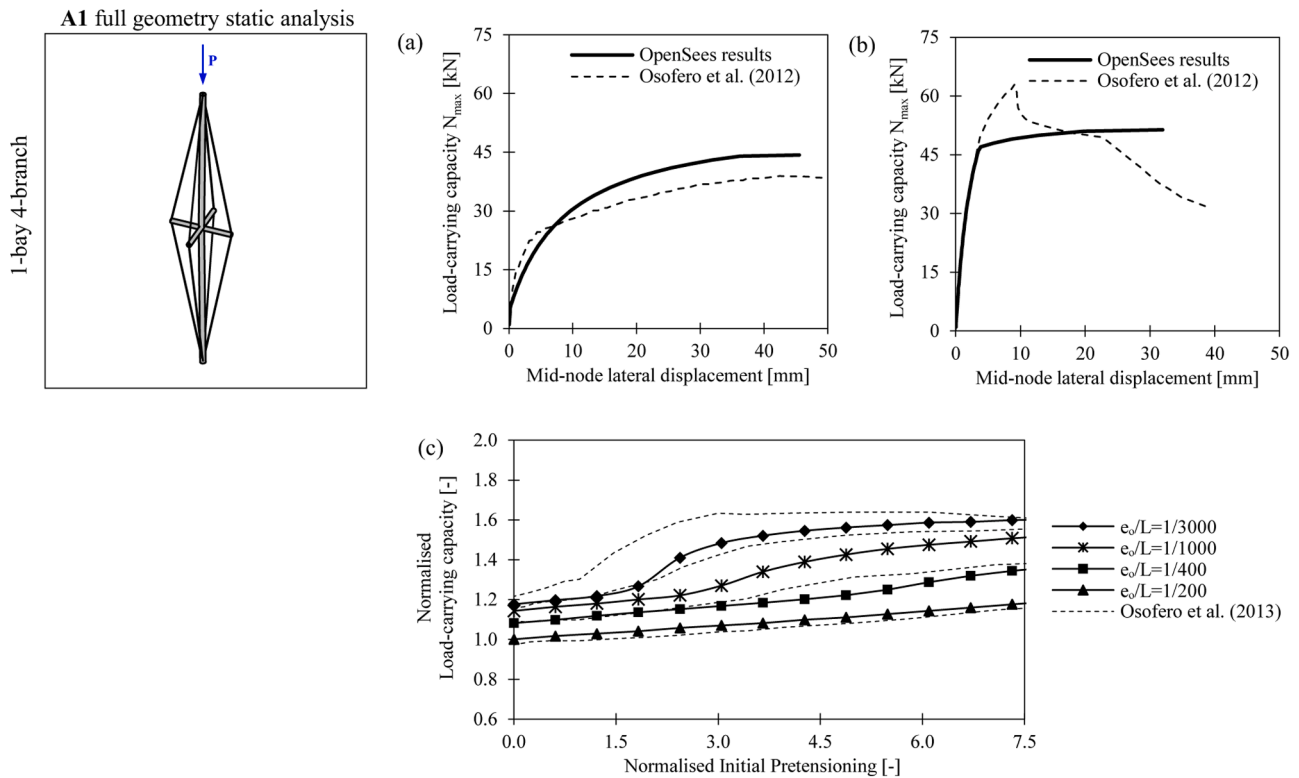

Fig. 5. Model validation of the cable-stayed column: comparison of numerical OpenSees model results against experimental results from Osofero et al., [53] for (a) case 2800 × 100-A1 where $T_0 = 1$ kN and (b) case 2800 × 100-A4 where $T_0 = 10.5$ kN; (c) comparison against the parametric numerical results from Osofero et al., [48] (case $2a/L = 0.05$), considering the variability of stay pre-tension and column imperfections.

modelling strategy.

The discrepancies in the validation results likely stem from a number of simplifications made in the OpenSees model. These were required to limit the computational effort and perform the large number of static and dynamic analyses conducted for the 67,500 configurations considered in the present study. Firstly, whilst material non-linearity is considered, this is done by assuming bilinear elasto-plastic or perfectly elastic material curves as discussed in Section 2.2. This study also limits the scope of considered shapes to the symmetric buckling mode by applying a single imposed global imperfection at the cross-arm locations. These assumptions might explain why the post-yield behaviour differs from that of the experimental results in Fig. 5a and 5b. Furthermore, the value of the pretensioning force in the cables may be somewhat lower than that assumed as part of the input parameters. This is because the calibration of cable pretensioning to account for end-shortening was omitted. This has an effect on the normalisation of the *x*-axis in Fig. 5c. The above simplifications should not adversely affect the insights stemming from the dynamic response of the cable-stayed columns under the cable-loss scenarios which is the main focus of this paper.

2.4. Sensitivity analysis on the baseline model

To understand the influence of individual parameters on the load-carrying capacity of the cable-stayed column (before cable loss is considered), an initial sensitivity study was conducted. This was carried out on the baseline model presented in Table 1-I, by performing quasi-static analyses. The influence of parameters was studied by varying the parameters, one-by-one, across a range of values, whilst keeping the other system parameters constant.

Fig. 6 summarises the results of this part of the study. The column and cross-arm member lengths were found to be the most critical

parameters. The results show that the system is still fundamentally governed by the column global buckling behaviour; hence, its response is strongly controlled by the column length (Fig. 6a). Moreover, the increase in cross-arm length (Fig. 6d) changes the angle of the stays' tensile force vectors, which in turn increases the magnitude of the lateral component of force restraining the column at the buckling point. As expected, the column's cross-section (*i.e.,* the second moment of area) also considerably affects the buckling capacity (Fig. 6b and 6c). Conversely, this initial analysis showed no observable difference when the second moment of area of the cross-arms was varied (*i.e.,* cross-arms diameter and wall thickness in Fig. 6e and 6f). The material and geometric properties of the cross-arm are such that for the considered ranges of parameters, stresses within the elements are minimal, and the material does not reach its yield limit. Similar observations were also made in previous studies (*e.g.,* [46,47]). Therefore, the influence of these parameters was deemed negligible for the multi-parameter analyses of the following Section 2.5. It is worth mentioning that this is rebuked further in the study, and further consideration of the cross-arm properties for cable loss simulations is given in Section 4.6. Changes to the stay diameter (Fig. 6g) were found to be as influential as the column cross-sectional properties. This parameter directly affects the level of stress within these elements. Bigger stays can carry larger forces; maintaining the same stay pre-tensioning leads to smaller values of initial strain. The stay pre-tension (Fig. 6h), as well as column imperfection levels (Fig. 6i), were found to have comparably limited influence. As stay pre-tension is primarily responsible for providing lateral restraint to the column, it was decided the effects of this parameter would be essential to study further within the multi-parameter analysis. On the other hand, for the sake of simplicity, it was decided to neglect the variability of the imperfection level.

A useful proxy that can quantify the level of sensitivity is the Sensitivity Ratio (SR), used in several fields with statistical applications
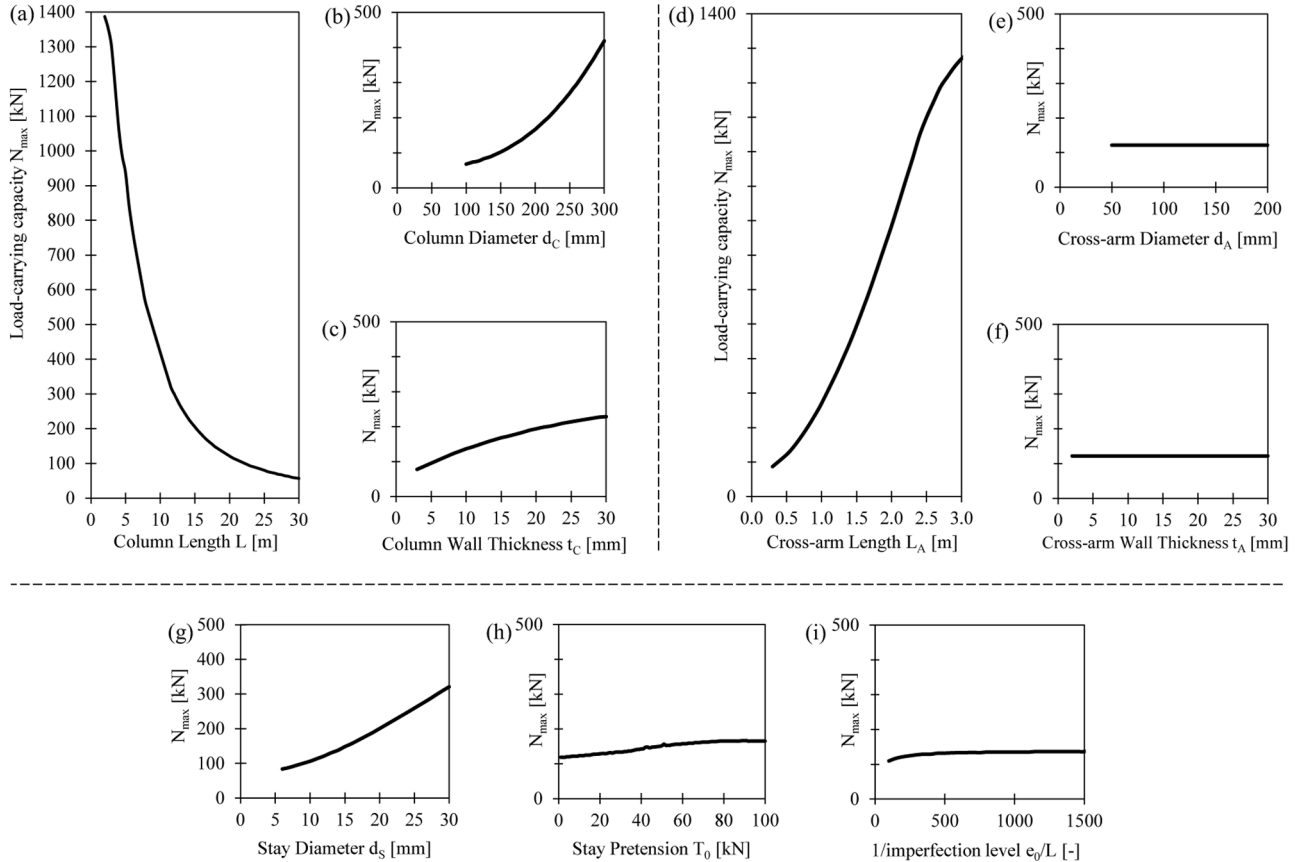

Fig. 6. Sensitivity analysis curves: load-carrying capacity plotted against the different parameters.

(*e.g.,* [69]). The SR is a measure of how much a result changes compared to the relative change in the base parameter; *e.g.,* an SR=2 means that a 10 % variation of the parameter induces a 20 % variation in the result. Fig. 7 shows the worst-case SRs evaluated for the different parameters considered in the baseline model. Comparing these values indicates how influential individual parameters are on the load-carrying capacity and supplements the abovementioned remarks. This analysis informed the key parameters and values of the multi-parameter analysis, as summarised in Table 1-II.

2.5. Multi-Parameter analysis

The multi-parameter analysis set out to determine the load-carrying capacities of various cable-stayed column configurations in a manner that captured the combined relationship of multiple parameters with the capacity. Alternative forms of certain parameters were derived to better represent the multi-parameter relationships.

Fig. 8 shows the results of the quasi-static analyses performed on cable-stayed columns considering the parameters summarised in Table 1-II. The load-carrying capacity is plotted against the non-dimensional slenderness ratio for four column configurations (*i.e.,* 1- and 2-bays with 4- and 6-branches). The Euler buckling curve shape remains prominent, and a clear exponential relationship between the capacity and non-dimensional slenderness ratio can be observed in all plots. Fig. 8 also shows regression curves for cases with cross-arm lengths corresponding to 0.3, 0.5 and 1.0 m; a clear distinction can be observed. Whilst the data for longer cross-arms is much more dispersed, the peak values, along with the pattern between the regression curves, indicate they can carry larger loads than systems with shorter cross-arms. This seems to have a larger impact than the overall geometrical configuration. Results of the 3- and 4-branch cases were found to be almost identical (hence, only 4-branch results were presented in Fig. 8). A difference was observed in 6-branch scenarios. This could imply that the system load-carrying capacity may not necessarily be driven just by the magnitude of the lateral restraining forces but rather by the number of restraining planes preventing lateral displacement of the node. This is an early indication that 6-branch configurations, subjected to stay loss, could retain a larger capacity than equivalent systems with fewer branches. Additionally, it can be observed that whilst a 2-bay configuration increased maximum capacities to a certain extent, the expansion of a 1-bay configuration to 6-branches was found most effective in increasing capacity.

To complement the analysis, steel tonnage requirements were measured by proxy of volume (this could be linearly expanded to estimate cost or embodied carbon). The scatter plot in Fig. 9a represents data from the parametric study for a 1-bay, 4-branch cable-stayed column system, illustrating the relationship between material tonnage and the load-carrying capacity. Regression curves are fitted through

groupings of columns with the same length. As expected, the material was found to be used most efficiently in shorter columns, where the buckling phenomenon is not as influential. In longer columns, it becomes more challenging to increase the column's capacity without significant increases to the steel tonnage. Naturally, the same could be said for typical columns (*i.e.,* without stays); however, the economy of *kg* of steel added for *kN* of capacity gained is superior for cable-stayed columns. Fig. 9b presents the tonnage results normalised in the context of equivalent standard columns, allowing a direct comparison of material savings between cable-stayed columns and conventional columns that are not tensioned. It was observed that cable-stayed columns are not effective in reducing material quantities within shorter column lengths. The presence of tensioned stays starts making an observable difference in columns that are 10 m or longer. Generally, material savings of up to 20 % can be achieved based on the analysed parametric cases. Linear formulas have been derived (included in Fig. 9b) to allow for a high-level estimate of steel tonnage required for a desired capacity (a numerical value in *kN* should be used to get a tonnage result in *kg*). A more general formula has also been determined for a variable column length (value of L in *m*):

$$m \approx \left(0.011\,L^2 - 0.17\,L + 1.03\right) \cdot N_{max} + 23.1\,L \qquad (1)$$

3. Analysis procedures for cable loss simulation

Cable loss scenarios were simulated by non-linear static and dynamic analysis following UFC guidelines [28]. The procedures are illustrated in Fig. 10 and were applied sequentially to individual cases. Rupture from accidental impact was deemed most likely for cable-stays closest to the column base; hence, the removal of the lowest cable on the side of the imposed imperfection was selected for collapse simulation; this would also generate the most conservative secondary moment in the column.

3.1. Non-linear static analysis

Static responses were first determined, as shown in Fig. 10a. A stayless geometry (A0) representing a traditional column is initially analysed along with the full geometry with cable-stays (A1) – these scenarios were covered in the previous sections of the study. The cable loss scenario in the static approach (A2) was carried out on a geometry where the relevant stay was not included in the analysis model. This approach effectively models the significant asymmetry of the system, including the imbalance of prestress in the stays. However, it does not account for the dynamic effects relating to instantaneous rupture.

Quasi-static analyses also provided the stiffness of the system (Fig. 10b), which, together with the mass, were used to estimate the natural frequency and later apply appropriate damping in the dynamic analyses. To capture the stiffness of the column more accurately, the initial end-shortening of the column tip as a result of the pre-tensioning
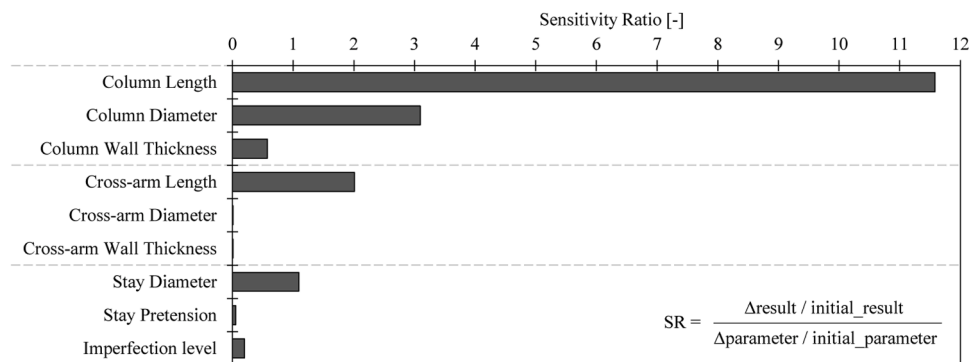

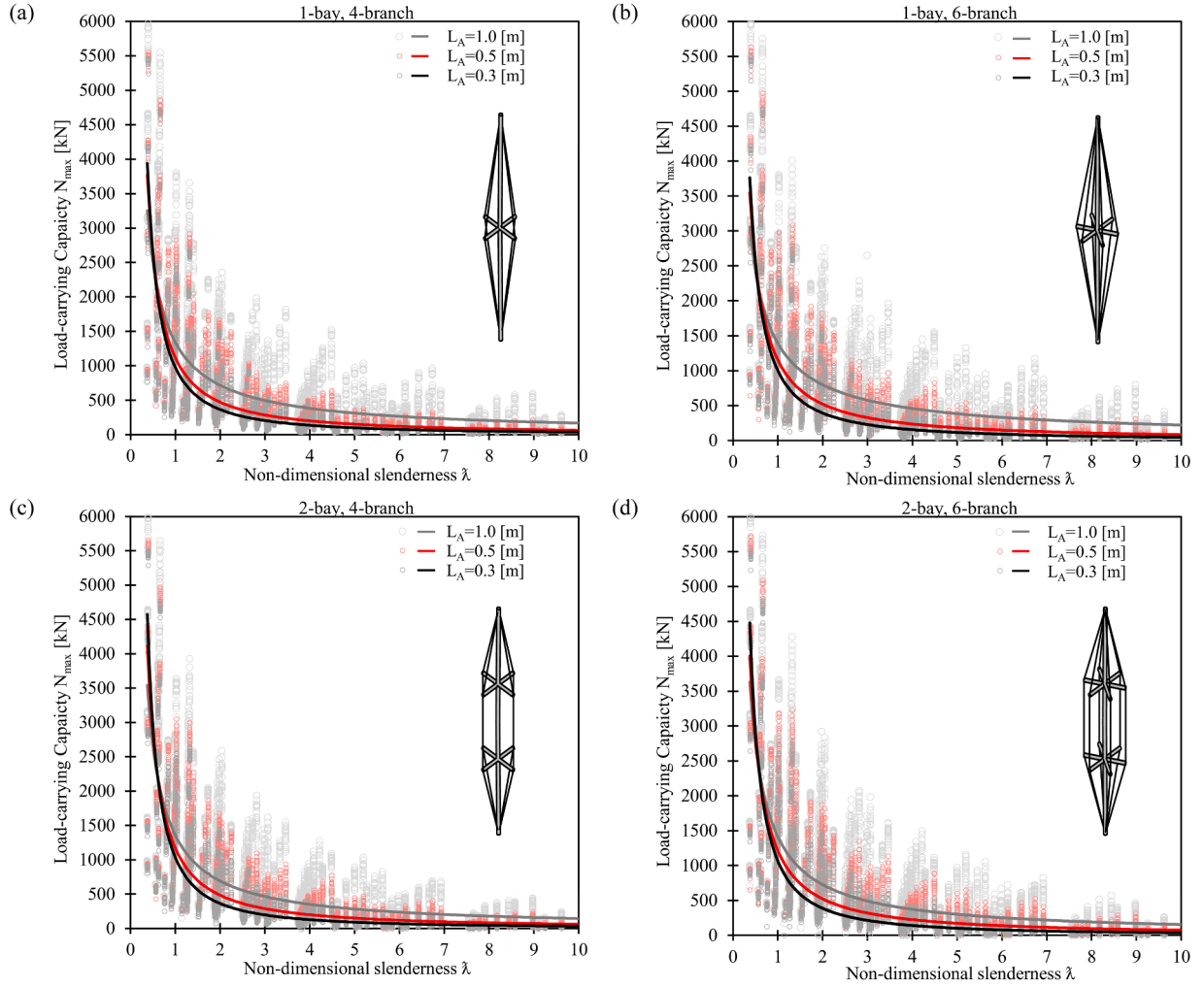**Fig. 7.** Sensitivity Ratios for the considered parameters.

Fig. 8. Load-carrying capacity results plotted against column non-dimensional slenderness ratio; results grouped by cross-arm length (L_A=0.3, 0.5 & 1.0 m) with regression curves; (a) 1-bay, 4-braches; (b) 1-bay, 6-braches; (c) 2-bay, 4-branches; (d) 2-bay, 6-braches.
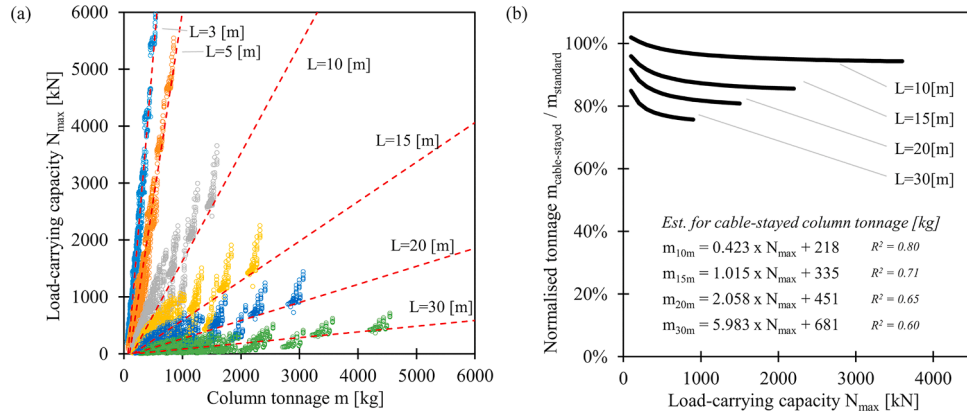

Fig. 9. (a) Column tonnage and achieved load-carrying capacity for full geometry cable-stayed column cases; (b) cable-stayed column tonnage normalised against equivalent standard column.

was measured (B1) and excluded from the vertical displacement of the top node used for the axial stiffness calculation (B2). The natural frequency was required to set an appropriate timestep for the subsequent analyses.

3.2. Non-linear dynamic analysis

To account for the dynamic effects of cable removal, non-linear time-history analyses were used. These relied on a removed-stay model geometry. The initial presence of the stay was simulated by imposing an equivalent set of tension forces. For 1-bay 4-branch configurations, these forces would be applied at the relevant cross-arm end and column base
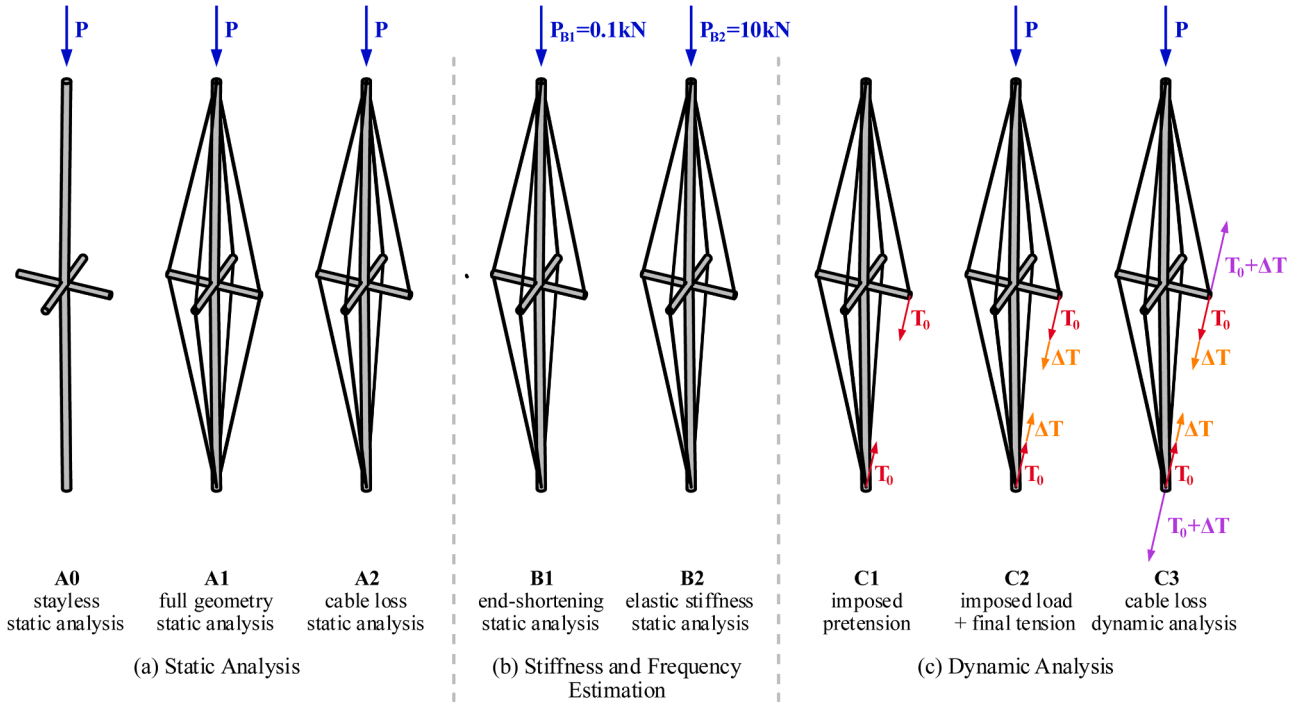
Fig. 10. Analyses procedures: (a) Quasi-static analysis; (b) Stiffness and natural frequency evaluation; (c) Dynamic analysis.

(Fig. 10c). The quasi-static analysis (Fig. 10a – A1) was used to determine the components of these force vectors. This approach allowed the stay to be emulated without being directly modelled as an element (Fig. 10c - C1). In addition to the initial pre-tensioning (T_0), a set of Δ_T forces was imposed to reflect the force change resulting from the application of the tip point load (Fig. 10c - C2).

The release of prestress in the cable is modelled by effectively imposing an equal and opposite set of nodal vector forces that equilibrate the initial prestress. This was simulated using a rise-time step forcing profile with loads equal and opposite to the sum of those applied earlier (Fig. 10c - C3). This load is incremented and rises to its full magnitude within the specified removal time, set to 10 % of the natural period of the system (following the recommendation of the GSA [70] for simulating instantaneous element removal). An imposed mass was determined coherently with the magnitude of the applied point load and was lumped at the column tip. Rayleigh Damping with a damping ratio ξ of 2 % was used.

Dynamic analyses were performed in an IDA fashion, increasing values of the applied force as done in Freddi et al. [21]. The time series for the dynamic analyses was set to a total of 10 times the natural period. The 'EnergyIncr' test in OpenSees [67] was used to handle convergence in the analysis. To improve convergence, a very fine default integration time step was set at 0.00005 s. A transient timestep procedure that adjusts the time step if convergence is not reached was implemented [21].

3.3. Engineering demand parameters (EDPs) and load factor coefficient (Γ)

A number of EDPs were monitored during the analyses. Whilst internal column axial forces were tracked, the column base reaction was used as a proxy for the load-carrying capacity. Fibre stresses in the columns and stays were recorded to assist in understanding the behaviour of the system. Vertical displacements of the top node, as well as lateral displacements of the middle node, were also monitored. It was found necessary to note the displacement of the cross-arm end node where cable loss would occur – this was crucial to specify load vectors

for the simulated stay presence and removal accurately.

Load factor coefficients (Γ) were used in the IDA as targets for the incremental load increase. For the purposes of this study, the coefficient Γ was simply taken as a normalisation of the applied load to the quasi-static load-bearing capacity of the cable-stayed column.

3.4. Dynamic increase factor (DIF)

The comparison between the non-linear quasi-static and dynamic analyses allows the definition of the DIFs. These are calculated as the ratio of the considered EDPs for the two types of analysis. The DIF indicates how much the static response would need to be amplified to capture dynamic effects and can be evaluated as follows:

$$DIF_R(\Gamma) = \frac{R_{dynamic}(\Gamma)}{R_{static}(\Gamma)}, \ DIF_N(\Gamma) = \frac{N_{dynamic}(\Gamma)}{N_{static}(\Gamma)}, \ DIF_U(\Gamma) = \frac{\delta_{dynamic}(\Gamma)}{\delta_{static}(\Gamma)} \quad (2)$$

where R, N, and δ are the base reaction (a proxy for load-carrying capacity), column axial force, and mid-node displacement, respectively. The DIFs are a function of Γ.

The study related to the evaluation of the DIFs is presented in Section 4.5.

4. Cable loss response

4.1. Quasi-static analysis

Fig. 11 shows the results of the quasi-static analysis (procedure A1 in Fig. 10a) of the baseline cable-stayed column (i.e., Table 1-I) with its full geometry before considering cable loss. Only results for the pinned cross-arm case are presented to explain the pre-rupture state. The load-carrying capacity was just under 120 kN (Fig. 11a). The pre-tensioning of the stays contributed to an initial internal axial force within the column, which increased with the applied load. The effects of buckling can be observed when investigating this parameter alongside the mid-node displacement (Fig. 11b). Once half the capacity was reached, the
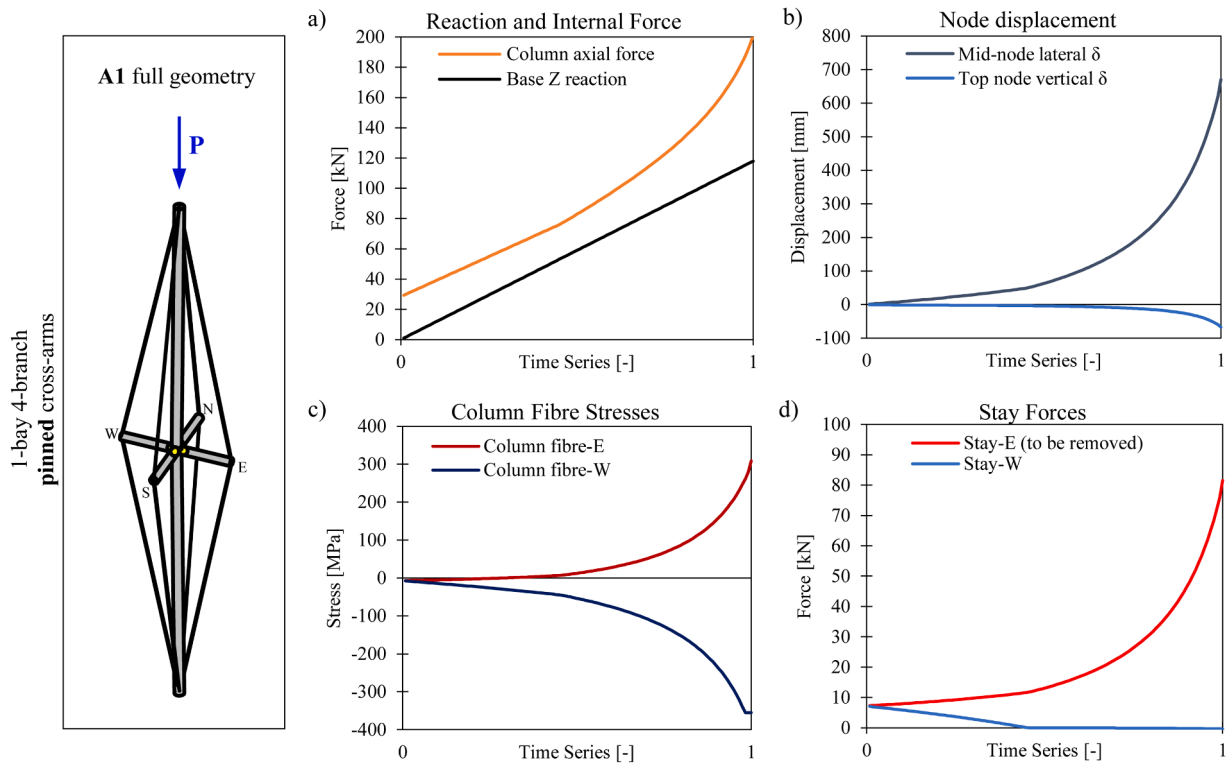
Fig. 11. Quasi-static analysis (A1) results of model geometry before cable loss for baseline 1-bay 4-branch configuration with pinned cross-arms.

column's deflection started to increase at a noticeable rate; considerable end-shortening also occurred right before the critical load was reached. These factors lead to the loss of stability of the column, resulting in collapse. The buckling behaviour of the column can be classed as inelastic as the column fibres began to yield before the critical load was reached (Fig. 11c). Considering the recorded cable stresses (Fig. 11d), it was found that at a certain point, stays on the opposite side of the deflection direction become ineffective; the column starts to rely primarily on the stays in the deflection direction, leading to a notable increase in their tensile stress. Similar considerations were also made in previous studies [45].

Fig. 12 shows the results of the same configuration in a quasi-static analysis (procedure A2 in Fig. 10a), but with the *stay-btm-E* removed (see Fig. 3b). For the model with pinned cross-arms, the capacity was substantially lower at about 70 kN (Fig. 12a). The upper stay, above the cable removal location, completely loses its pre-tensioning due to the flexibility of the connection between the cross-arm and column (Fig. 12d). This results in the column having no beneficial restraint against buckling at mid-height. Furthermore, the now unbalanced pretensioning on the opposite side accelerates the phenomenon. A higher load-carrying capacity of 85 kN was reached in the fixed cross-arm model (Fig. 12e). It is stipulated that the bending stiffness of the cross-arm allows the upper stay to continue providing some lateral restraint, as observed by the tensile force increase of the stay (Fig. 12h). This also resulted in a differential of internal axial force within the upper and lower halves of the column (Fig. 12g).

Table 2 shows a summary of the obtained quasi-static load-carrying capacities for the abovementioned cases alongside results for a stayless column (analysis A0). The presence of the pre-tensioned cables clearly contributed to an increase in capacity (analysis A1) by >70 %. In the instance where pinned-cross arms were applied (analysis A2-pinned), the loss of a stay reduced the capacity to comparable levels of a typical (non-pretensioned) column. In the fixed-cross arm case (analysis A2-fixed), the capacity was also greatly reduced; however, this remained approximately 20 % larger than the pinned case.

4.2. Load-carrying capacity increase potential and reduction under cable loss

The results from Section 4.1 were replicated for alternative bay/branch configurations and normalised against the load-carrying capacity of the fundamental non-pretensioned column geometry (A0). This normalisation allows for quantification of the capacity increase benefits of the cable-stay system and the capacity reduction under a cable loss scenario. Results provided in Fig. 13 continue to represent the baseline geometrical properties set out in Table 1-I.

Considering the benefits of the full cable-stayed system before cable rupture (A1), capacities were found to increase by at least 75 % for the considered configurations compared to the stayless column (A0). There was no significant distinction between the performance of columns with pinned or fixed cross-arms in 1-bay, 3- and 4-branches configurations; fixed-cross arms achieved a noticeably higher performance in the 6-branches and 2-bay configurations. 6-branches systems were found to have the largest capacity increase effect, likely due to the additional restraining planes and larger overall pre-tensioning of the column. In the cable loss scenarios (A2), any capacity benefits of the cable-stayed systems were eradicated for configurations with pinned cross-arms, except for 6-branch systems, which maintained about 20 % capacity over the non-pretensioned column (A0). Conversely, a larger residual capacity was achieved by fixed cross-arm columns for all configurations; the capacity increases (A0 to A1) were noticeably higher, and the drop under cable loss (A1 to A2) was not as severe as with the pinned cases. The smallest reductions were recorded for 6-branch cases, further highlighting the benefits of this configuration.

These quasi-static analyses were expanded onto a larger pool of cases with different geometrical properties, as presented in Fig. 14, where parameters defining the system geometry were sequentially varied from the baseline. Analogous conclusions can be drawn, thus indicating the general validity of the previous statements relating to the effects of the system's configuration and cross-arm restraints on the redundancy of the system subject to cable loss. In all cases, the use of pinned cross-arms
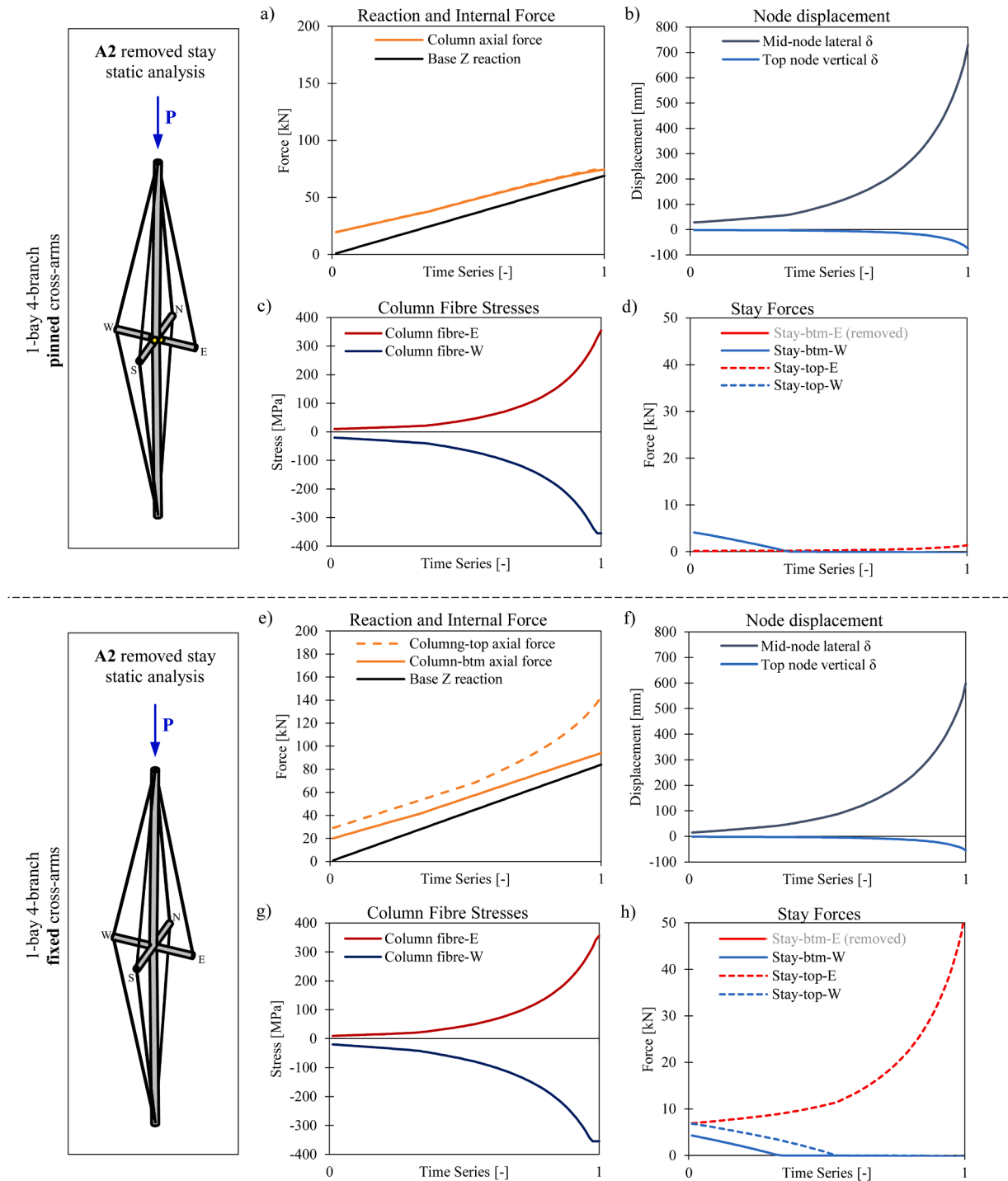
Fig. 12. Quasi-static analysis (A2) results of cable loss for baseline 1-bay 4-branch configuration with pinned cross-arms (a) to (d) and fixed cross-arms (e) to (h).

Table 2
Quasi-static capacities of baseline 1-bay 4-branch cable-stayed column – comparison of stayless, full cable-stayed and cable loss scenarios.

Analysis		Load-carrying capacity [kN]
A0	Standard stayless column	68
A1	Full cable-stayed column geometry	118
A2	Removed stay, pinned cross arms	69
A2	Removed stay, fixed cross-arms	84

significantly affects the system's residual load-carrying capacity, which reduces to levels comparable to a stayless column. Only 6-branch cases were found to retain some level of increased capacity under cable loss. Systems with higher levels of initial pre-tensioning are characterised by lower capacity after a cable rupture event (Fig. 14f). Fixed cross-arms appear to provide a better redistribution of forces with the loss of a stay, although this heavily depends on the specific geometry of the system. The higher the benefit of the increased load-carrying capacity of a column, the larger the capacity reduction it may face under cable loss (easily observed for longer cross-arm lengths in Fig. 14d). It is stipulated that the cross-arm deflection can lead to the reduction of the lateral
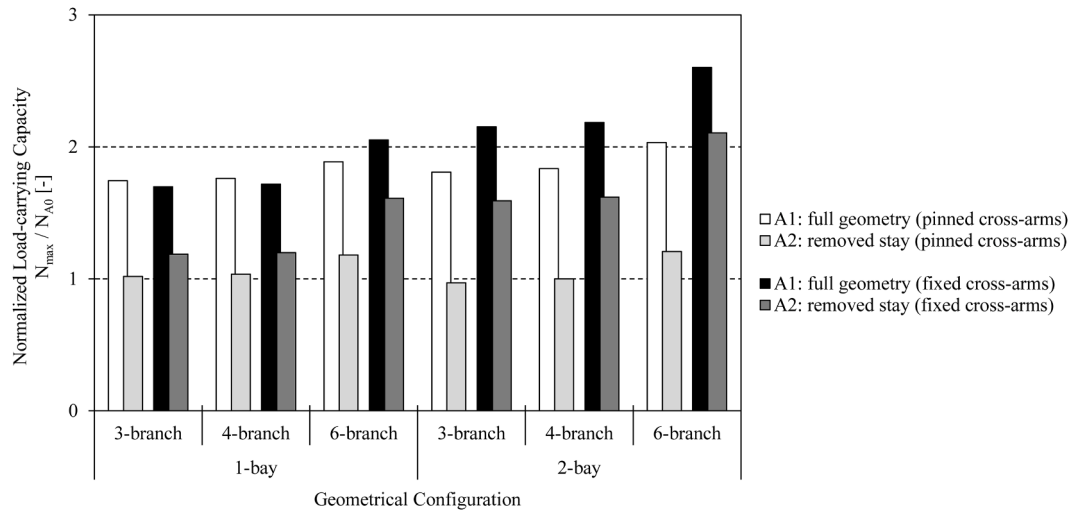
Fig. 13. Normalised load-carrying capacities for various geometrical configurations of the baseline cable-stayed column and static stay loss models.

restraining component of the pre-tensioning force in the upper stay, thus amplifying unfavourable effects and accelerating buckling.

4.3. Dynamic analysis

Dynamic effects relating to sudden cable failure typically amplify the system's response. Hence, when these effects are considered, peak demands are higher than those obtained by quasi-static analyses. The response eventually settles to that indicated by the quasi-static analysis after the dynamic effects have damped out.

Fig. 15 shows the dynamic response of the baseline 1-bay 4-branch case with a 50 kN point load subjected to cable loss for cases with pinned and fixed cross-arms.

The pinned cross-arm model (Fig. 15a-d) shows a peak reaction response of 59 kN, *i.e.*, about 20 % higher than the load originally applied. Simultaneously with the removal of the lower stay, its upper equivalent suffers a complete loss of pre-tensioning due to the lack of cross-arm fixity. At the end of the removal period, the column records its lowest axial force, as the column effectively *springs up* as the pre-tensioning is lost. With the system mass in motion, the column begins to deflect considerably further than it would under a static force. Once the peak response is reached, the behaviour of the cable-stayed column becomes oscillatory, and damping effects are observed.

A similar response was obtained in the fixed cross-arm simulation (Fig. 15e-h). In this case, the system responded equivalently to a static load of 56 kN, which is closer to the original load value. Recorded peak displacements were about half that of the pinned case. The beneficial effects from the cable above the location of rupture can be observed - the bending stiffness of the cross-arm allowed the stay to partially sustain its pre-tensioning. As with the findings of the static analysis, the upper half of the column was subjected to a higher axial force. The effects of this can also be observed in the column fibre stress recordings.

Interestingly, the observed system responses were not perfectly sinusoidal – elongated peaks and sharper troughs were noticed in both models, but most prominently in the pinned cross-arm case where the column's response reached closer to its buckling limit. This behaviour is attributed to the variable stiffness of the system during the dynamic motion of the column. The effects of pre-tensioning, in conjunction with the deflection of the column after rupture, cause the remaining stays on the opposite side to come in and out of tension irregularly in time. These elements do not take loads in compression, and therefore, the rate of their strain changes when the tensile force reduces to zero.

This stiffness variation is more evident in the pinned cross-arm cases. This may also be due to the negative consequences of second-order effects, which are increased as a result of the change in the position of the stays and cross-arms in the transverse plane. This occurs since the simulated pinned connection of the cross-arms allows them to deflect laterally (in plan). As a result, their restraining capabilities are reduced not only due to a decrease in tensile force but also as the deflected position of the stays now contributes to further lateral deflection of the column. This is investigated further in Section 4.6.

4.4. Incremental dynamic analyses (IDAs)

IDAs were used to evaluate the variation in dynamic response for increasing loads. Fig. 16 shows the results of the IDAs for the baseline model, where the values of the load factor Γ were iteratively increased. The response for $\Gamma=0.1$ indicated a good match with the natural period of the system predicted in the initial calculations; for larger loads, the inelastic period is higher than the estimated elastic period due to the system's non-linear behaviour.

The pinned cross-arm model (Fig. 16a and 16b) was loaded up until $\Gamma\approx0.5$. The peak mid-node lateral deflection was found to roughly double each time the factor went up by 10 % increments. An increase in the natural period followed a similar pattern. Whilst the peak reaction value was also found to increase, it did not increase at the same rate as observed for the other parameters. Furthermore, the non-standard harmonic response, *i.e.*, the previously mentioned elongations of peaks, can be much more clearly observed for higher load factors.

Fig. 16c and 16d present a similar pattern of results for the fixed cross-arm model, which was successfully analysed up to $\Gamma\approx0.45$. In this case, the peak value of deflection was far more limited. Increases in the recorded reactions were similar to the pinned case, but the peak elongations observed previously were much less prominent. The higher natural frequencies of the system were noticeable, justified by a larger overall stiffness due to the cross-arm fixity.

4.5. Dynamic increase factors (DIFs)

The system's response under cable-stay loss scenarios should account for the dynamic effects. However, dynamic analyses are often complex and have a high computational cost. A more convenient, widely used strategy is based on quasi-static analyses where the dynamic effects are indirectly considered by amplifying the static loads through the DIF.

The IDA procedure presented in the previous section was applied to the full range of considered bay/branch configurations and for a selection of non-dimensional slenderness ratios, evaluated as $\bar{\lambda} = \sqrt{Af_y/N_{cr}}$ [68]. DIFs were evaluated for the established EDPs: mid-node lateral
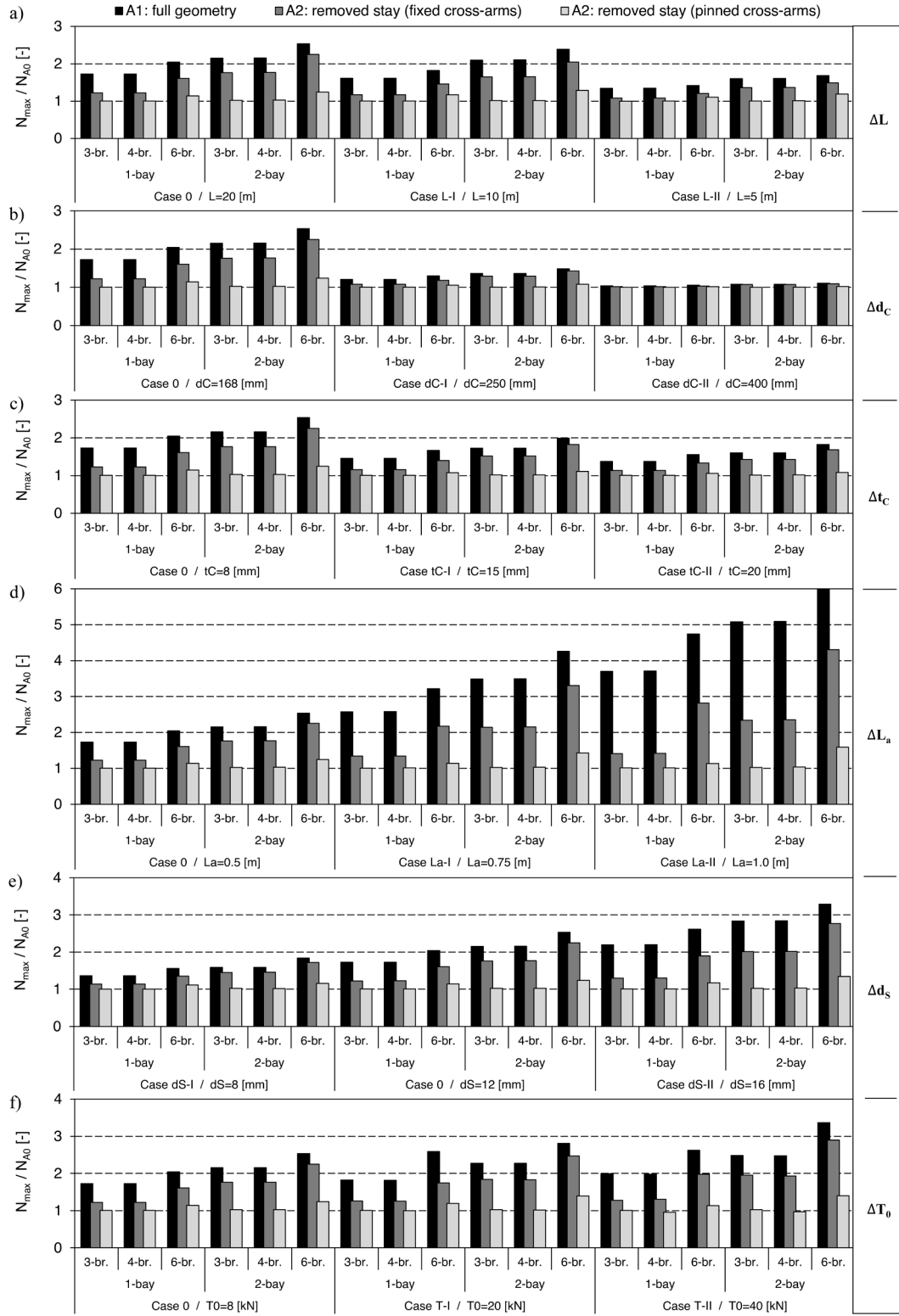
Fig. 14. Normalised load-carrying capacities of cable-stayed columns and static stay loss models for various geometrical configurations; geometry parameter values adjusted from the baseline model.

displacement, vertical reaction, and column axial load.

The first series of results in Fig. 17 present DIFs for the baseline column, which is characterised by a high non-dimensional slenderness ratio (*i.e.,* $\bar{\lambda} = 4.6$, where the elastic critical buckling load is *ca.* 21 times smaller than its uniform compression strength). The results for alternative bay/branch configurations, using the same baseline parameters,

are also plotted. Curves are fitted to grouped data to obtain functions that could be used to estimate the DIF.

The formulas below are proposed as appropriate general expressions. An exponential curve was found to best represent the *DIF-U* for displacement, whilst logarithmic and power functions were judged to be the best fits for *DIF-N* (axial force) and *DIF-R* (reaction), respectively.
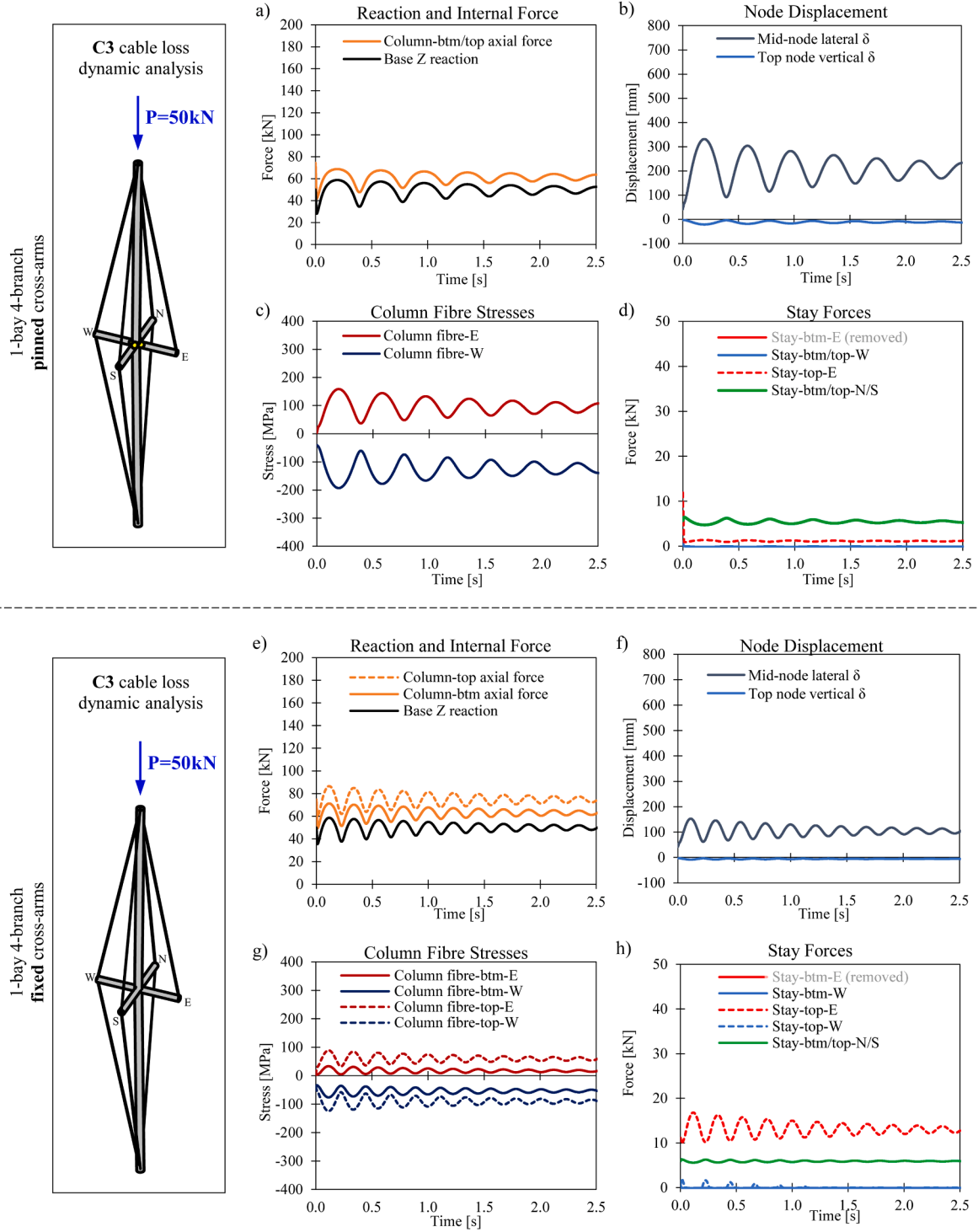
Fig. 15. Dynamic analysis results of cable loss for the baseline 1-bay 4-branch configuration with pinned cross-arms (a) to (d) and fixed cross-arms (e) to (h); response under 50 kN point load at column tip.

Coefficients for the fitted curves in Fig. 17 are provided in Table 3.

$$DIF_U = a \cdot e^{(b\Gamma)} \quad , \quad DIF_R = a \cdot \Gamma^{(b)} \quad , \quad DIF_N = a \cdot ln(\Gamma) + b \qquad (3)$$

Generally, in the pinned cross-arm case (Fig. 17a-c), DIFs for 1- and 2-bay configurations were found to be similar; hence, trendlines for individual branch typologies were plotted, encompassing both 1- and 2-bay geometries. The results indicate the dynamic mid-node displacement response of the cable-stayed columns could be as much as 1.5–2 times larger than a static analysis would predict (Fig. 17a). For internal

axial force and base reaction, the curves indicated the DIFs tend towards 1.1–1.2 for the highest load factors (Fig. 17b and 17c). Configurations with 3- and 4-branches were determined to have the highest DIFs for all EDPs. Results for 6-branch cases performed best, resulting in the lowest DIF.

In the fixed cross-arm model (Fig. 17d-f), a distinction can be made between 1- and 2-bay configurations; results for all 2-bay geometries were grouped as these were found to be similar. The determined DIFs are lower than the previously analysed cases. The highest differences can be
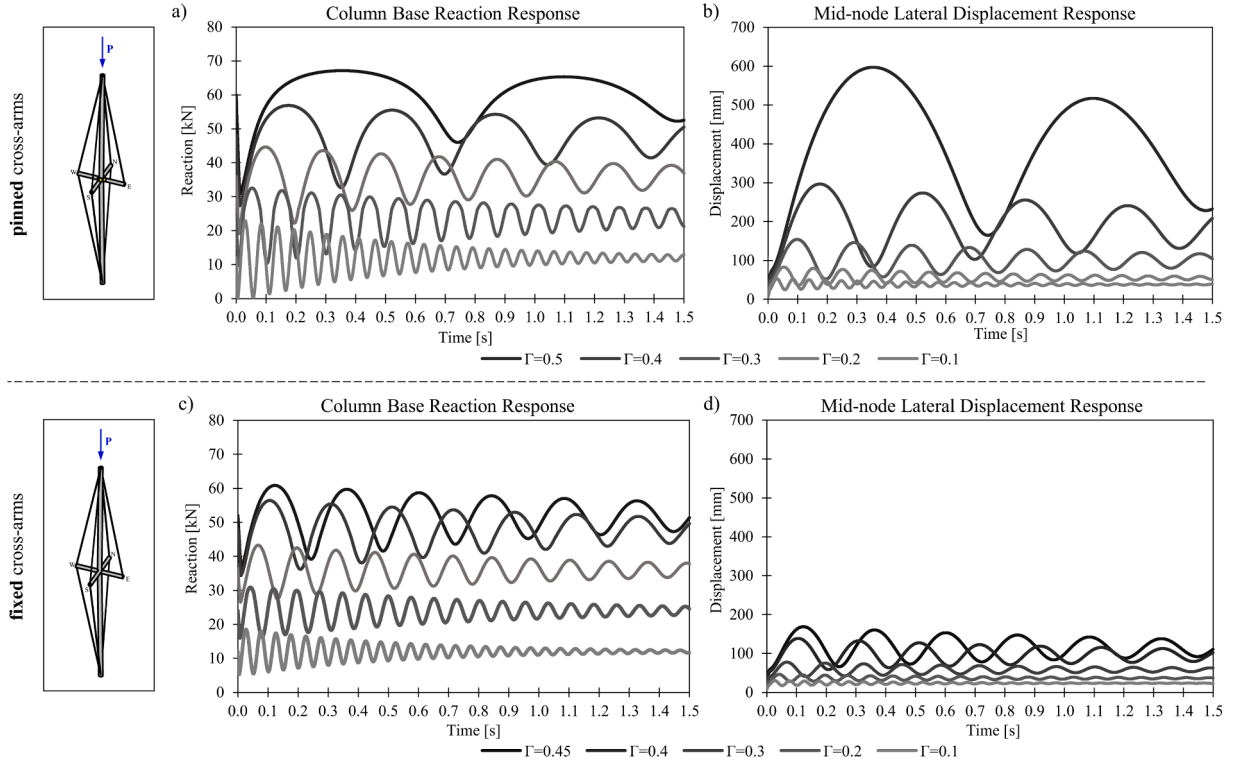
Fig. 16. Incremental Dynamic Analyses (IDAs) of cable loss for the baseline 1-bay 4-branch configuration with pinned cross arms (a) to (b) and fixed cross-arms (c) to (d); load factors associated with the load-carrying capacity of the full geometry stayed-column.
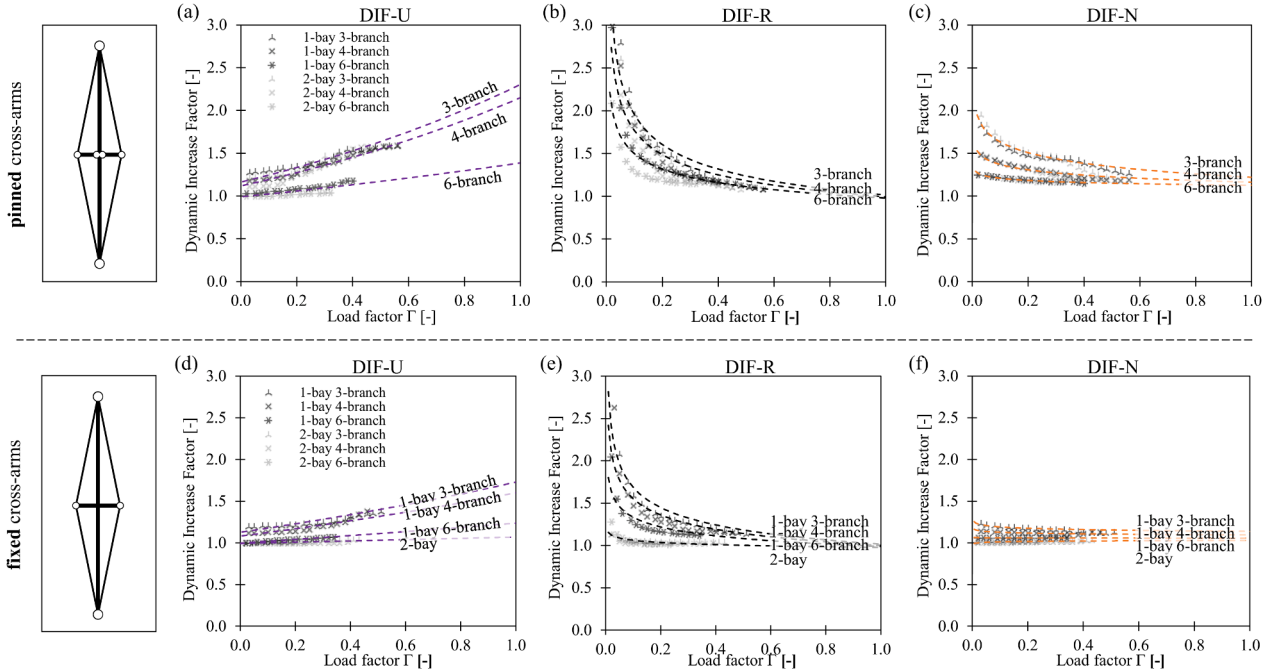

Fig. 17. Dynamic Increase Factors (DIFs) for cable loss for various geometric configurations of the baseline column ($\lambda = 4.6$) with pinned cross-arms (a) to (c) and fixed cross-arms (d) to (f).

observed in terms of dynamic mid-node displacement (Fig. 17d) and internal axial force (Fig. 17f). Smaller differences can be observed for the base reaction (Fig. 17e).

The second series of DIF results are presented in Fig. 18. These plots provide a comparison of 1-bay 4-branch columns with different non-dimensional slenderness ratios for pinned and fixed cross-arm models; this was carried out by varying the column length and outer diameter

from the baseline properties. The plots show a clear pattern – the DIF increases with the non-dimensional slenderness of the column. Similarly, the results show that columns with an elastic critical force close to the compressive resistance (*i.e.,* low slenderness) have negligible dynamic effects. Table 4 provides the regression coefficients for the fitted curves in Fig. 18.

Table 3
Regression coefficients for data in Fig. 17.

Cross-arm configuration	Geometry	DIF	a	b
pinned cross-arms	3-branch	DIF_U	1.1632	0.6832
		DIF_R	1.0159	−0.284
		DIF_N	−0.179	1.2201
	4-branch	DIF_U	1.1174	0.6542
		DIF_R	0.9945	−0.25
		DIF_N	−0.09	1.163
	6-branch	DIF_U	0.9898	0.3368
		DIF_R	0.9796	−0.185
		DIF_N	−0.036	1.1268
fixed cross-arms	1-bay, 3-branch	DIF_U	1.1275	0.4268
		DIF_R	1.0145	−0.221
		DIF_N	−0.023	1.1377
	1-bay, 4-branch	DIF_U	1.0807	0.3922
		DIF_R	0.9995	−0.191
		DIF_N	−0.014	1.0949
	1-bay, 6-branch	DIF_U	0.9976	0.2144
		DIF_R	0.9875	−0.13
		DIF_N	−0.001	1.0568
	2-bay	DIF_U	0.9935	0.0738
		DIF_R	0.9761	−0.036
		DIF_N	0.0073	1.0288

4.6. Influence of cross-arm bending stiffness and deflection

The findings of previous static and dynamic analyses comparing pinned and fixed cross-arm models found obvious differences that affected the behaviour of the cable-stayed column subject to cable loss. A hypothesis was drawn that the bending stiffness of the cross-arm could be detrimental in providing redundancy to the system in the event of sudden cable rupture. The negative effects of cable loss in a stayed column with pinned cross-arms (or with a low bending stiffness) can be better understood when comparing the shape of the displaced column against a column with stiff cross-arms. Fig. 19a presents the deflected shapes of the baseline cases previously evaluated. The stiffer cross-arm scenario can provide more restraining benefits than more deformable cross-arms. The more the cross-arms deflect away from the direction of buckling, the smaller the lateral restraining force becomes on the buckling side, whilst the resultant forces on the opposite side increase, further propagating the mid-node deflection; this is particularly noticeable in 3- and 4-branch columns.

The influence of the bending stiffness was studied further by increasing the diameter of the cross-arm profile; the results of a quasi-static analysis are presented in Fig. 19b. Almost identical results were obtained for 3- and 4-branch systems; hence, these are grouped into a single curve. Cross-arms with a low bending stiffness (as simulated earlier by the pinned cross-arm model) have lower load-carrying capabilities under a cable loss scenario. The analysis also showed that, in order to achieve a capacity increase benefit from cross-arm fixity, there is a minimum bending stiffness (EI) requirement that maximises the effectiveness of the cross-arms. For the analysed baseline case, this was found to be *ca.* 1000 kNm^2 – an increase in the bending stiffness past this value had a minimum effect on the capacity for the considered configurations.

The above considerations imply that progressive collapse resistance in cable-stayed columns could be improved by ensuring an appropriate cross-arm profile and connection fixity. The cross-arm would need to sufficiently resist bending both vertically (from the pre-tensioned stay that remains in the same plane where the cable has ruptured) as well as laterally (as the cross-arms deflect away from the buckling direction). This capacity could be further improved by implementing a 6-branch configuration.

Alternative cross-arm arrangements could enable better performance following the cable loss scenario. Fig. 20a presents a single-plane system with double cross-arms. Inclining the cross-arms vertically could sustain a larger lateral restraining component of the pre-tensioned stay that remains in the event of cable loss; such a system would require a separate stability system out-of-plane. The system in Fig. 20b shows a typical cable-stayed column configuration fitted with additional elements acting as a ring beam tying the cross-arms together. This solution does not affect the original load-carrying capacity but could significantly improve the system's performance under stay loss. The ring beam increases the cross-arm stiffness and greatly reduces the vertical and lateral displacements of the branches, thus allowing them to retain beneficial effects for higher loads. Such solutions have been
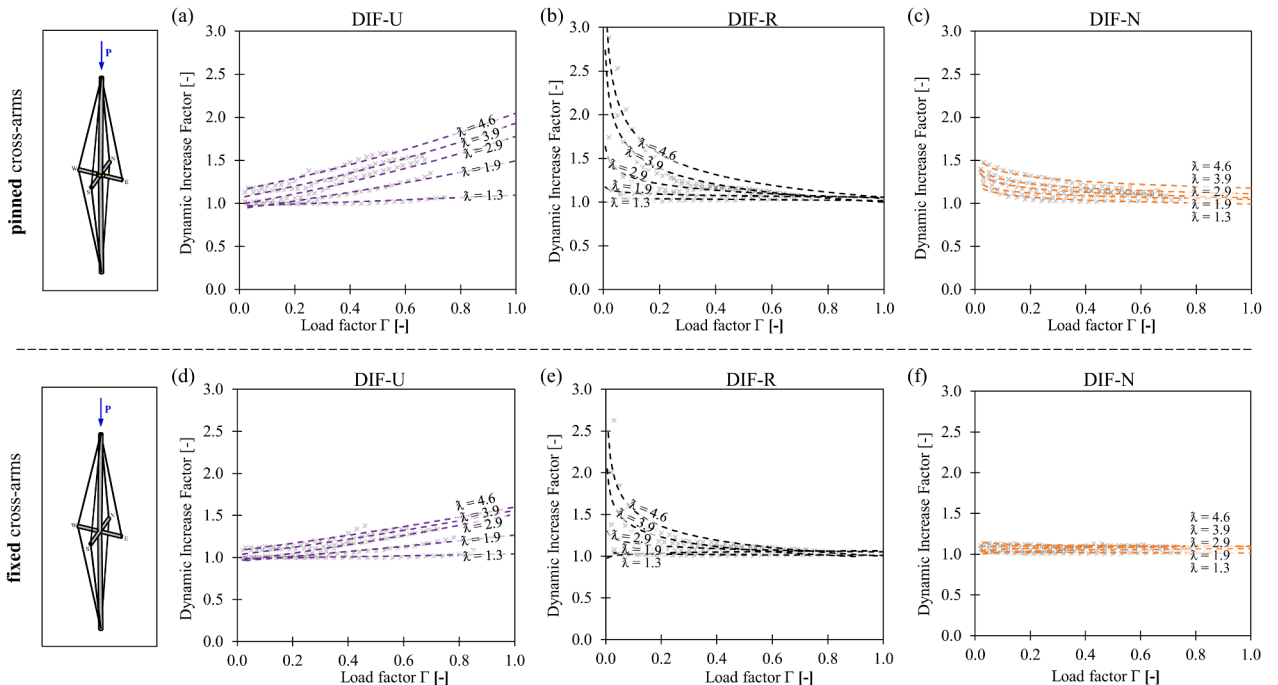

Fig. 18. Dynamic Increase Factors (DIFs) for cable loss of 1-bay 4-branch configuration for various non-dimensional slenderness ratios; pinned cross-arms (a) to (c) and fixed cross-arms (d) to (f).

Table 4
Regression coefficients for the data in Fig. 18.

| Geometry	λ	DIF	a	b	Geometry	λ	DIF	a	b
1-bay, 4-branch pinned cross-arms	4.6	DIF_U	1.1511	0.5772	1-bay, 4-branch fixed cross-arms	4.6	DIF_U	1.0807	0.3922
		DIF_R	1.0546	−0.24			DIF_R	0.9995	−0.191
		DIF_N	−0.082	1.1789			DIF_N	−0.014	1.0949
	3.9	DIF_U	1.0659	0.5949		3.9	DIF_U	1.03	0.4157
		DIF_R	1.0001	−0.203			DIF_R	0.98	−0.141
		DIF_N	−0.072	1.1124			DIF_N	0.0002	1.098
	2.9	DIF_U	0.9872	0.5898		2.9	DIF_U	0.9579	0.4586
		DIF_R	1.0459	−0.09			DIF_R	1.0499	−0.041
		DIF_N	−0.07	1.0661			DIF_N	0.0149	1.0952
	1.9	DIF_U	0.937	0.467		1.9	DIF_U	0.9558	0.282
		DIF_R	1.0556	−0.021			DIF_R	1.0645	0.0164
		DIF_N	−0.047	1.0471			DIF_N	0.0189	1.0672
	1.3	DIF_U	0.9678	0.1238		1.3	DIF_U	0.9854	0.056
		DIF_R	1.0125	−0.016			DIF_R	1.0103	−0.008
		DIF_N	−0.05	0.9923			DIF_N	−0.004	1.0143
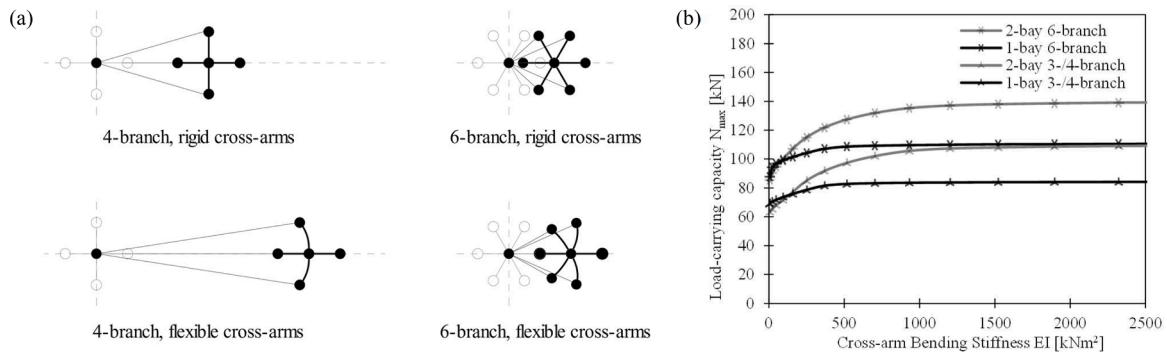
Fig. 19. (a) Plan view of cable-stayed column mid-height displacements for 4- and 6-branch configurations; comparison of pinned and fixed cross-arm cases. (b) Relationship of load-carrying capacity to the bending stiffness of the cross-arms for various geometrical configurations in static removed stay analyses, baseline case.
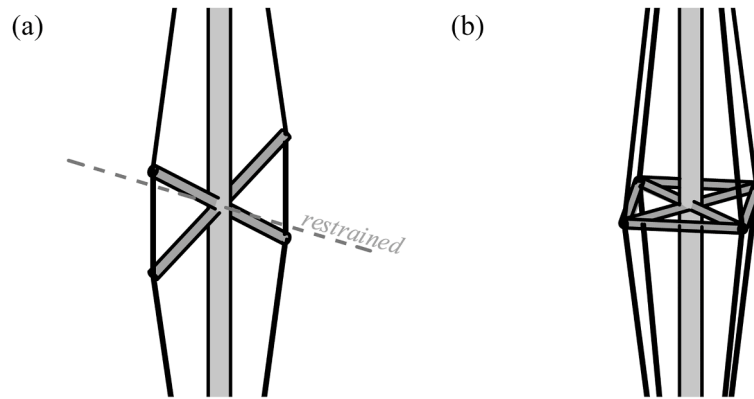

Fig. 20. Alternative cable-stayed column designs that could be more resistant to progressive collapse.

implemented in some pioneering works, such as the "Rock in Rio III" stadium in Rio de Janeiro, Brazil [45,71].

5. Conclusions

This study examines the robustness of cable-stayed columns under various cable loss scenarios. Different bay/branch configurations, featuring fixed and pinned cross-arms, were analysed using Finite Element (FE) models in OpenSees, incorporating both material and geometric non-linearities. A comprehensive parametric study assessed the impact of key variables on load-carrying capacity. Non-linear quasi-static and dynamic analyses simulated cable loss scenarios, and

Incremental Dynamic Analyses (IDAs) were used to determine Dynamic Increase Factors (DIFs) across several slenderness ratios. The following conclusions have been drawn:

1. The sensitivity study highlighted key factors affecting load-carrying capacity. Column and cross-arm lengths had the greatest impact: longer columns significantly reduced the critical buckling load, while longer cross-arms enhanced the lateral restraint from stay pre-tensioning. Column cross-sectional properties and stay diameter also played important roles. Stay pre-tensioning and imperfection levels had limited influence in the studied cases. While cross-arm cross-

sectional properties were insignificant under normal loading, they proved critical in stay loss scenarios.

2. The multi-parameter analysis revealed the simultaneous effects of various parameters on different bay/branch configurations. The 3- and 4-branch configurations exhibited similar load-carrying capacities, which significantly increased with 6-branch configurations. When comparing material requirements for fabrication, the configurations showed minimal differences, as most material is concentrated in the main column element. The analysed cases showed that material tonnage savings of up to 20 % can be achieved compared to traditional columns.

3. Detailed quasi-static analysis results for the baseline 1-bay 4-branch column under cable-stay loss scenarios were presented, considering both fixed and pinned cross-arms. In all cases, column capacity was significantly reduced due to stay loss. For columns with pinned cross-arms, any beneficial capacity increases were removed or worsened by initial pre-tensioning, except for 6-branch configurations, which retained some residual capacity. Systems with fixed cross-arms performed better, though capacity reductions remained significant.

4. Dynamic time-history analyses revealed significant dynamic effects from sudden cable rupture. IDAs evaluated system responses at various load levels for different bay/branch configurations and columns with varying slenderness. DIFs were estimated for mid-node lateral displacement, column axial force, and base vertical reaction. Columns with higher slenderness had larger DIFs, while fixed cross-arm scenarios showed lower factors.

5. The effects of cross-arm bending stiffness and deflection on system robustness were investigated. Pinned cross-arms resulted in the weakest capacity, as deflection in the buckling direction accelerated the buckling process. Increasing cross-arm stiffness improved load capacity, with the highest potential in 6-branch configurations. However, beyond a certain point, further increases in stiffness were ineffective, suggesting optimal cross-section properties for maximum robustness with minimal material. Alternative cable-stayed column forms were proposed to resist progressive collapse.

This study offers general insights into the performance and design of cable-stayed columns under scenarios involving cable loss and highlights several open questions. Future research should experimentally evaluate cable-loss scenarios to enhance modelling validation under both static and dynamic conditions. Additionally, studies should explore performance under multi-cable loss scenarios and focus on developing innovative configurations to improve system robustness, promoting the definition of detailed design recommendations.

CRediT authorship contribution statement

Michał Kierat: Writing – original draft, Investigation, Formal analysis, Data curation, Conceptualization. **Fabio Freddi:** Writing – review & editing, Supervision, Methodology, Investigation, Conceptualization.

Declaration of competing interest

The authors declare that they have no known competing financial interests or personal relationships that could have appeared to influence the work reported in this paper.

Data availability

Data will be made available on request.

References

[1] ASCE 7-10, Minimum Design Loads for Buildings and Other Structures, American Society of Civil Engineers, Reston, Virginia, USA, 2013.

[2] C. Pearson, N. Delatte, Ronan Point apartment tower collapse and its effect on building codes, J. Perf. Constr. Facil. 9 (2) (2005) 172–177.

[3] M.A. Sozen, C.H. Thornton, W.G. Corley, P.F. Mlakar, The Oklahoma City bombing: structure and mechanisms of the Murrah building, J. Perf. Constr. Facil. 12 (3) (1998) 120–136.

[4] Z.P. Bažant, M. Verdure, Mechanics of progressive collapse: learning from World Trade Center and building demolitions, J. Engin. Mech. 133 (3) (2007) 308–319.

[5] M. D'Antimo, M. Latour, G. Rizzano, J.F. Demonceau, Experimental and numerical assessment of steel beams under impact loadings, J. Constr. Steel Res. 158 (2019) 230–247.

[6] F. Dinu, I. Marginean, D. Dubina, I. Petran, Experimental testing and numerical analysis of 3D steel frame system under column loss, Eng. Struct. 113 (2016) 59–70.

[7] J.M. Adam, M. Buitrago, E. Bertolesi, J. Sagaseta, J.J. Moragues, Dynamic performance of a real-scale reinforced concrete building test under a corner-column failure scenario, Eng. Struct. 210 (2020) 110414.

[8] N. Stathas, I. Karakasis, E. Strepelias, X. Palios, S. Bousias, M.N. Fardis, Tests and analysis of RC building, with or without masonry infills, for instant column loss, Eng. Struct. 193 (2019) 57–67.

[9] M. Buitrago, J. Sagaseta, N. Makoond, A. Setiawan, J.M. Adam, Robustness of a full-scale precast building structure after edge column failure, Eng. Struct. 326 (2025) 119495.

[10] S.-B. Kang, K.H. Tan, Progressive collapse resistance of precast concrete frames with discontinuous reinforcement in the joint, J. Struct. Engin. 143 (9) (2017) 04017090.

[11] R. Zandonini, N. Baldassino, F. Freddi, Robustness of steel-concrete flooring systems. An experimental assessment, Stahlbau 83 (9) (2014) 608–613.

[12] R. Zandonini, N. Baldassino, F. Freddi, G. Roverso, Steel-concrete composite frames under the column loss scenario: an experimental study, J. Constr. Steel Res. 162 (2019) 105527.

[13] G. Roverso, N. Baldassino, R. Zandonini, F. Freddi, Experimental assessment of an asymmetric steel-concrete frame under a column loss scenario, Eng. Struct. 293 (2023) 116610.

[14] B.A. Izzuddin, A.G. Vlassis, A.Y. Elghazouli, D.A. Nethercot, Progressive collapse of multi-storey buildings due to sudden column loss – Part I: simplified assessment framework, Eng. Struct. 30 (2007) 1308–1318.

[15] A.G. Vlassis, B.A. Izzuddin, A.Y. Elghazouli, D.A. Nethercot, Progressive collapse of multi-storey buildings due to sudden column loss – Part II: application, Eng. Struct. 30 (2007) 1424–1438.

[16] A. Francavilla, M. Latour, G. Rizzano, Ultimate behaviour of bolted T-stubs under large displacements: a mechanical model, J. Constr. Steel Res. 195 (2022) 107355.

[17] D. Stephen, D. Lam, J. Forth, J. Ye, K.D. Tsavdaridis, An evaluation of modelling approaches and column removal time on progressive collapse of building, J. Constr. Steel Res. 153 (2019) 243–253.

[18] C. Dimopoulos, F. Freddi, T.L. Karavasilis, G. Vasdravellis, Progressive collapse of self-centering moment resisting frames, Eng. Struct. 208 (2020) 109923.

[19] A.F. Santos, A. Santiago, M. Latour, G. Rizzano, Robustness analysis of steel frames subjected to vehicle collisions, Structures 25 (2020) 930–942.

[20] M. Scalvenzi, S. Gargiulo, F. Freddi, F. Parisi, Impact of seismic retrofitting on progressive collapse resistance of RC frame structures, Engin. Fail. Anal. 131 (2022) 105840.

[21] F. Freddi, L. Ciman, N. Tondini, Retrofit of existing steel structures against progressive collapse through roof-truss, J. Constr. Steel Res. 188 (2022) 107037.

[22] L. Possidente, F. Freddi, N. Tondini, Dynamic increase factors for progressive collapse analysis of steel structures considering column buckling, Engin. Fail. Anal. 160 (2024) 108209.

[23] A.G. Vlassis, B.A. Izzuddin, A.Y. Elghazouli, D.A. Nethercot, Design oriented approach for progressive collapse assessment of steel framed buildings, Struct. Eng. Int. 16 (2) (2006) 129–136.

[24] D. Stevens, B. Crowder, D. Sunshine, K. Marchand, R. Smilowitz, E. Williamson, M. Waggoner, DoD research and criteria for the design of buildings to resist progressive collapse, J. Struct Eng. 137 (9) (2011) 870–880.

[25] N. Hoffman, U. Kuhlmann, J.F. Demonceau, J.P. Jaspart, N. Baldassino, F. Freddi, R. Zandonini, Robust impact design of steel and composite building structures: the Alternate load Path approach, in: *Safety, Robustness & Condition Assessments of Struct., Workshop 2015*, IABSE, Helsinki, Finland, 2015.

[26] GSA, Progressive collapse analysis and design guidelines for new federal office buildings and major modernisation project, *General Services Administration*, Washington, DC, 2003.

[27] CEN, EN, Eurocode 1: Actions on structures – Part 1–7: General actions – Accidental actions, 1991–1–7, European Committee for Standardization, Brussels, Belgium, 2006.

[28] DOD, Unified Facilities Criteria (UFC) – design of structures to resist progressive collapse, *United States Department of Defense*, UFC 4-023-0314 – Change 3, Arlington, Virginia, 2016.

[29] M. Byfield, W. Mudalige, C. Morison, E. Stoddart, A review of Progressive Collapse research and regulations, Inst. Civ. Eng. 167 (8) (2014) 447–456.

[30] J.M. Adam, F. Parisi, J. Sagaseta, X. Lu, Research and practice on progressive collapse and robustness of building structures in the 21st century, Eng. Struct. 173 (2018) 122–149.

[31] F. Otto, Tensile structures-cable structures, II, MIT Press, 1969.

[32] Y. Liu, B. Han, M. Xiao, Advances in progressive collapse of bridge structures, Pac. Sci. Rev. 13 (3) (2011) 173–181.

[33] U. Starossek, Progressive collapse of bridges - aspects of analysis and design, in: Int. Symposium on Sea-Crossing Long-Span Bridges, 2006, pp. 1–22.

[34] D. Malomo, N. Scattarreggia, A. Orgnoni, R. Pinho, M. Moratti, G.M. Calvi, Numerical study on the collapse of the Morandi Bridge, J. Perf. Constr. Facil. 34 (4) (2020) 04020044.

[35] TTSB (2020). Final report on Nanfangao Sea-crossing bridge collapse. https://www.ttsb.gov.tw/english/16051/16113/16114/28249/post.

[36] J.C. Morales, L.E. Suárez, Collapse of the arecibo observatory In puerto rico: reflections from a structural engineering perspective, Rev. Int, Desastres Nat. Accid. Infraestruct. Civ. 19-20 (1) (2021).

[37] S. Krishnan, Cable-stayed columns and their applications in building structures, J. Build, Eng. 27 (2020) 100984.

[38] ARUP, Arup J. 146 (2) (2011) 3–20.

[39] K.-H. Chu, S.S. Berge, Analysis and design of struts with tension ties, J. Struct., Div. 89 (1) (1963).

[40] H.R. Mauch, L.P. Felton, Optimum design of columns supported by tension ties, J. Struct., Div. 93 (3) (1967).

[41] M.C. Temple, Buckling of stayed columns, J. Struct., Div. 103 (4) (1977).

[42] H.H. Hafez, M.C. Temple, J.S. Ellis, Pretensioning of single-crossarm stayed columns, J. Struct., Div. 105 (2) (1979) 359–375.

[43] K.C. Wong, M.C. Temple, Stayed column with initial imperfection, J. Struct Div. 108 (7) (1982).

[44] M.C. Temple, M.V. Prakash, J.S. Ellis, Failure criteria for stayed columns, J. Struct., Eng. 110 (11) (1984) 19293.

[45] D. Saito, M.A. Wadee, Post-buckling behaviour of prestressed steel stayed columns, Eng., Struct. 30 (5) (2008) 1224–1239.

[46] D. Saito, M.A. Wadee, Numerical studies of interactive buckling in prestressed steel stayed columns, Eng., Struct. 31 (2) (2009) 432–443.

[47] D. Saito, M.A. Wadee, Buckling behaviour of prestressed steel stayed columns with imperfections and stress limitation, Eng., Struct. 31 (1) (2009) 1–15.

[48] A.I. Osofero, M.A. Wadee, L. Gardner, Numerical studies on the buckling resistance of prestressed stayed columns, Adv., Struct., Engin. 16 (3) (2013) 487–498.

[49] P. Li, X. Liu, C. Zhang, Interactive buckling of cable-stiffened steel columns with pin-connected crossarms, J. Constr., Steel Res. 146 (2018) 97–108.

[50] K. Wu, M.A. Wadee, L. Gardner, Interactive buckling in prestressed stayed beam-columns, Int, J. Mech, Sci. 174 (2020) 105479.

[51] K. Wu, X. Qiang, Z. Xing, X. Jiang, Buckling in prestressed stayed beam–columns and intelligent evaluation, Eng, Struct. 255 (2022) 113902.

[52] R.R. de Araujo, S.A.L. de Andrade, Silva da, P.C.G. Vellasco, J.G.S. da Silva, L.R. O. de Lima, Experimental and numerical assessment of stayed steel columns, J. Constr., Steel Res. 64 (9) (2008) 1020–1029.

[53] A.I. Osofero, M.A. Wadee, L. Gardner, Experimental study of critical and post-buckling behaviour of prestressed stayed columns, J. Constr., Steel Res. 79 (2012) 226–241.

[54] M. Serra, A. Shahbazian, L.S. daSilva, L. Marques, C. Rebelo, P.C.G. da Silva Vellasco, A full scale experimental study of prestressed stayed columns, Eng, Struct. 100 (2015) 490–510.

[55] G. Lv, P. Li, C. Zhang, X. Sun, E. Chen, Experimental investigation into the buckling behaviour of cable-stiffened steel columns, J. Constr, Steel Res 183 (2021) 106753.

[56] J. Shen, R.M.J. Groh, M.A. Wadee, M. Schenk, A. Pirrera, Probing the stability landscape of prestressed stayed columns susceptible to mode interaction, Eng, Struct. 251 (2022) 113465.

[57] J. Shen, L. Lapira, M.A. Wadee, L. Gardner, A. Pirrera, R.M.J. Groh, Probing *in situ* capacities of prestressed stayed columns: towards a novel structural health monitoring technique, Phil Trans. R Soc. (2023). A.38120220033.

[58] D. Saito, M.A. Wadee, Optimal prestressing and configuration of stayed columns, Inst., Civ. Eng., 163 (5) (2010) 343–355.

[59] L. Lapira, M.A. Wadee, L. Gardner, Stability of multiple-crossarm prestressed stayed columns with additional Stay systems, Structures 12 (2017) 227–241.

[60] J. Yu, M.A. Wadee, Mode interaction in triple-bay prestressed stayed columns, Int., J. Non-Linear Mech. 88 (2017) 47–66.

[61] J. Yu, M.A. Wadee, Optimal prestressing of triple-bay prestressed stayed columns, Structures 12 (2017) 132–144.

[62] K. Wu, M.A. Wadee, L. Gardner, Prestressed stayed beam-columns: sensitivity to prestressing levels, pre-cambering and imperfections, Eng, Struct. 226 (2021) 111344.

[63] M.A. Wadee, L. Gardner, A.I. Osofero, Design of prestressed stayed columns, J. Constr., Steel Res. 80 (2013) 287–298.

[64] K. Wu, Z. Xing, G. Li, H. Chang, Fire behavior of prestressed stayed columns: critical temperature and mode transition, J. Struct., Engin. 150 (5) (2024) 04024038.

[65] K. Wu, Z. Xing, H. Li, Nonlinear stability and design of prestressed stayed columns in fire considering non-uniform temperature distribution, J. Build., Eng. 79 (2023) 107807.

[66] R.R. de Araujo, J.G. da Silva, P.C.S. Vellasco, S.A. de Andrade, L.R. de Lima, L. A. Simões da Silva, Non-linear dynamic analysis of stayed steel columns, Inter, Colloq. Stab. Ductility Steel Struct. 1 (2010) 423–430.

[67] Mazzoni S., McKenna F., Scott M.H., Fenves G.L., Open System for Earthquake Engineering Simulation User Command-Language Manual, OpenSees version 2.0, 2009.

[68] EN 1993–1–1. Eurocode 3: design of steel structures – Part 1–1: general rules and rules for buildings, Brussels, Belgium, 2005.

[69] J. Clavreul, D. Guyonnet, T.H. Christensen, Quantifying uncertainty in LCA-modelling of waste management systems, Waste Manag. 32 (2012) 2482–2495.

[70] GSA, Alternate path analysis and Design guidelines for progressive collapse resistance, *General Services Administration*, Washington, DC, 2013.

[71] S.A.L. de Andrade, Vellasco PCGdaS, J.G.S. da Silva, Concepcao e projecto estrutural do palco principal do Rock in Rio III, Constr. Mag. 6 (2003) 4–11 [in Portuguese].